Anonymous Referee #3

The manuscript analyzes seven field campaigns where particle number size distributions (PNSD) and sulfur dioxide were measured at the summit of a mountain site in the North China plain. Supporting measurements of time-resolved PM2.5, O3, and oxides of nitrogen were taken. And each campaign included 1-h time resolution ions in PM2.5 using water extractive methods (URG-AIM or MARGA). The most recent campaign was in 2018. Across the 7 campaigns, a little over 100 particle formation and growth events were detected, with the analysis focused on the size range of 10-300 nm size range. From the earliest to most recent campaign, SO2 emissions and concentrations have dropped dramatically, and the paper tries to analyze whether the particle formation and growth activity has changed in ways that are expected from the sulfur dioxide decrease. A large number of metrics are computed and then analyzed for each particle formation and growth event (PFGE). The metrics include, but are not limited to, the apparent formation rate of 10-25 nm particles (FR), the growth rate, the absolute increase in N10-25 particle concentration from the start to the peak of the PFGE (this is the NMINP variable), the PFGE duration, the PFGE frequency, the size to which the growth event reaches (Dpgmax variable in the manuscript), and particle counts which are used as surrogates for the change in CCN concentrations at low, medium, and high supersaturations (N100-300, N80-300, and N50-300). The paper includes values for and discussion of total VOC during the campaigns.

Complicating the analysis is that the field campaigns were in different months of the year: April 2007 (~30 d), June 2009 (~20 d), Aug 2014 (~30 d), Oct/Nov 2014 (~70 d), Jul 2014 (~40 d), Dec 2017 (~35 d), and Mar 2018 (~30 d).

The paper's abstract makes five claims: a. The formation rate in 2018 is 2-3 times higher than the formation rate in 2007. b. Net maximum increase in nucleation mode number concentration is 2-3 times higher in 2018 than in 2007. c. The occurrence of events where the mode of the growth event goes above 50 nm is lower in 2018 than it was in 2007. d. A surrogate for CCN production at high supersaturation (N50-300 at its peak during each growth event minus N50-300 before the event) decreased from 3703 per cm3 (before 2015) to 1026 (2017-2018). e. The authors argue availability of organic precursors has increased in the most recent campaigns, allowing more particle production and initial growth; furthermore, they argue that the lack of later growth is from reduction of "anthropogenic precursors" (presumably SO2).

The paper requires substantial revision before it is suitable for publication. The key issue, to this reviewer, is that making accurate claims about year-on-year trends and variability in PFGE is difficult. The requirements to make the claims defensible are: (1) take a sufficient number of samples to reduce random variability and give sufficient statistical power; (2) take steps to minimize, test for, and quantify campaign-specific systematic instrument bias (also known as "instrument drift"); (3) take steps to enforce consistency in any subjective data interpretation steps, such as classification of PFGE into "types" and the determination of the start and end times of events; (4) use statistical methods designed for trend analysis, time series analysis, and combined analysis of seasonal and interannual variability.

Each requirement needs to be met in order for the claims about trends to be defensible. And for

peer review and reproducibility purposes, things need to be documented for the peer-review and scientific communities.

I think the current work fails to meet all four of the requirements. While some of the conclusions are likely accurate (in that they would not change if all the requirements were met) – others would change, or require extensive qualification.

Response: Thanks for the review's constructive comments. We agree that some analyses and related conclusions in our original version should be more conservative. In addition, more clarifications are needed to better defense them. Scientific community normally prefers to see the extracted trend in ambient variables using the measurement data over 20 years. Thus, the technical term "trend" used in the original version is problematic and has be removed.

Long-term continuous measurements may allow better investigating NPF trends, however, all statistical tools in literature suffer from the weakness to some extent in extracting the de-weathered trend in interested variables associated with anthropogenic perturbation, based on our previous studies. For non-continuous measurements, it is still a common challenge to address specific scientific questions using the proper statistical analysis. We thereby remove the technical "trend" through the whole manuscript in the revision.

A comparative analysis was conducted to study particle formation and growth events (PFGE) in different years based on two observational facts, 1) their occurrence frequencies in 2007 and 2009 were reasonably same as those in 2017 and 2018 even in different seasons; 2) a large decrease in SO_2 mixing ratio 2017 and 2018 against in 2007 and 2009. We then focused on comparative analyzing the spring PFGEs in 2007 and 2018, when uncertainties from varying ambient factors may have been largely minimized. This has been clarified in the revision.

We also found a large variation in occurrence frequency of summer PFGEs in different years. For the summer PFGEs, it may require extremely abundant chemical information to study the effect of decreasing SO_2 levels on PFGEs because of a huge perturbation from meteorological conditions and related biogenic emissions of air pollutants. On the other hand, the observations of summer PFGEs also implied that the same occurrence frequencies of PFGEs may be a critical indicator to constrain the comparative analysis.

We highly appreciate the comments on technical issues of measurements. The commercial instruments were routinely calibrated to ensure the QA/QC using the service provided by their vendors. We agree that more cautions should be paid to instrument limitations, especially in a small particle size range. In the following text, we try our best to address the comments point by point and revise the manuscript accordingly, in order to improve our analysis more defensible and robust. Please note that after the major revisions of our manuscript, we have also made substantial changes in this response, and the language-editing have been processed in this version.

1. Statistical power:

PFGE exhibit substantial seasonal variation, due to changes in temperature, relative humidity,

biogenic activity, atmospheric chemistry, soil moisture, preexisting aerosol concentration and chemistry, radiation, cloudiness, boundary layer structure, land cover/vegetation canopy structure, synoptic meteorology, anthropogenic emissions, and atmospheric ion levels. Local meteorological features (i.e. orographic meteorology) and local sources may also have month-to-month variability. And at the 20-30 d time scale, large scale persistent geophysical features can cause a whole campaign of measurements to be atypically high or low for a number of PFGE variables. To accommodate all these sources of variability, large sample sizes are required for analysis of seasonal variation and interannual trends. In the absence of large sample sizes, careful pairing of events and analysis of alternate sources of variability / alternate hypotheses are needed isolate cause-effect relationships on specific PFGE variables.

With each campaign at a slightly different time of the year, some campaigns as short as 20 d, and no discussion of whether air pollution levels, air pollution meteorology, and climate variables were at climatologically representative levels, the reader has to apply great skepticism to any claims of interannual trends and cause-effect relationships for those interannual trends. See for example (Birmili and Wiedensohler 2000) who do take into account air mass characteristics.

Response: To our best understanding from recent review papers on PFGE, eight variables, i.e., concentrations and cumulative generation amounts of sulfuric acid together with Highly Oxygenated Organic Molecules (HOM) and other secondary organics in different volatilities, the product of gaseous HNO_3 and gaseous NH_3 minus the equilibrium constant of NH_4NO_3 and then minus the kelvin effect term, cumulative generation amounts of condensed NH_4NO_3 on size-dependent particles, would directly affect apparent new particle formation rate (FR), apparent net maximum increase in the nucleation-mode particle number concentration (NMINP), new particle growth rate (GR) and the maximum geometric median diameter of grown new particles (D_{pgmax}). Although gaseous amines have been proposed to participate in ambient nucleation, their concentrations in China, based on the authors' work, are too high (relative to sulfuric acid) to act as the limitation factor. How aminium salts contribute the growth of newly formed particles larger than 10 nm is poorly understood in China, which is out of scope of this study. What the reviewer claim above may indirectly affect the eight variables to some extent. Only the information of the eight variables is not sufficient to support our analysis, those indirect factors should be cautiously utilized to facilitate the analysis. The arguments have been clarified in the revision (e.g., lines 40-44, lines 242-247, lines 341-345).

We agree that the technical term "trend" is misleading and has been removed in the revision. We also revised our discussion on the cause-effect relationships of PFGE by considering significant changes in the eight variables (lines 434-449).

In polluted and NH_3-rich (we may reasonably assume that amines may also be rich relative to sulfuric acid) ambient air in China, the influence of air mass characteristics on PFGE may be totally different from that in the clean and pristine atmospheres. In clean and pristine atmospheres, air mass characteristics may provide important information on precursors' sources of PFGE. In China, precursors of PFGE are abundant in general. For example, the occurrence frequency of PFGE reached ~50% in winter campaign as presented in this study, while the value was less than 5-10% in winter in Europe. Alternatively, air mass characteristics greatly affect moisture

characteristics and may subsequently affect the cloudiness (radiation) and H_2SO_4 concentration through modulating OH free radical concentration. Of course, the latter is poorly studied so far.

The size distributions shown in Figure S3 are suggestive of insufficient number of days sampled in the dataset. Telling whether the system shifted from unimodal to bimodal behavior between 2015 and 2017 (all unimodal for 2015 and prior) vs. this occurring through some instrument drift vs. this occurring through sampling non-climatological conditions due to small samples sizes is difficult.

Given the decrease (Table 2) in PM2.5, sulfate, and SO2 between spring 2007 and 2018 (PM2.5 60 vs. 30 ug/m3; sulfate 17 vs. 4 ug/m3, SO2 18 vs. 3 ppb), more discussion is needed of the large increase in condensation sink in 2018 (Figure S3) and in the large increase in the height of the size distribution function at 100 and 150 nm between 2007 and 2015.

The discontinuity in the slope of the size distribution function at 200 nm also indicates there may be some drift in the size-specific performance of the WPS (Figure S3). The discontinuity in slope is not really evident until 2017, but then appears in 2017 and 2018.

Response: We agree that the analysis of PFGE in the origin version misses out the important point. On the light of the comments, we re-checked the data. We do find that three channels in WPS around 213 nm suffered from unexpected errors in reporting number concentrations in approximately 30% sampling days in 2017 and 2018. It has a minor influence on PFGE in 7 NPF days out of the total of 32 NPF days in 2017 and 2018 as shown in Fig. S4 in the revised supplementary materials. The data in the three channels suffering from abnormal errors will be corrected by assuming a linear decrease of particle number concentration from 150 nm size bin to 300 nm size bin. Thank again.

We plotted particle number size distributions on non-NPF days in different years (Figure R1). Bimodal particle number size distributions can be observed in 2009, 2014 and 2015. We don't see any shift when the size distributions in 2014, 2015 and 2018 were compared with each other. We also find that the median geometric diameters of accumulation mode on NPF days in 2017 were consistent with those on non-NPF days in 2014, 2015 and 2018. However, the median geometric diameters of accumulation mode on non-NPF days in 2017 did shift to the large size and the same was true for those on non-NPF days in 2009. Moreover, the median geometric diameters of accumulation mode on NPF days in 2009 were consistent with those on non-NPF days in 2014, 2015 and 2018. Overall, our regular instrument maintenance appears to be effective to prevent from the instrument shift, except the occasional problem at three size bins around 213 nm.

In the origin manuscript, we calculated condensation sink based on the different size range of particle in 2007 (10-153 nm) and 2018 (10-300 nm). To be consistent, we recalculated CS based on 10-153 nm particles on 2018, and the average of 0.40 ± 0.15 s^{-1} was slightly larger than the average CS in 2007 (0.32 ± 0.19). CS should be unrelated to secondary particles via ambient nucleation since the particles cannot grow over 60 nm. Primary emissions of the accumulation mode particles were out of scape of this study, although they may scavenge precursors of PFGE to

some extent. This has been added in revision, lines 371-373.

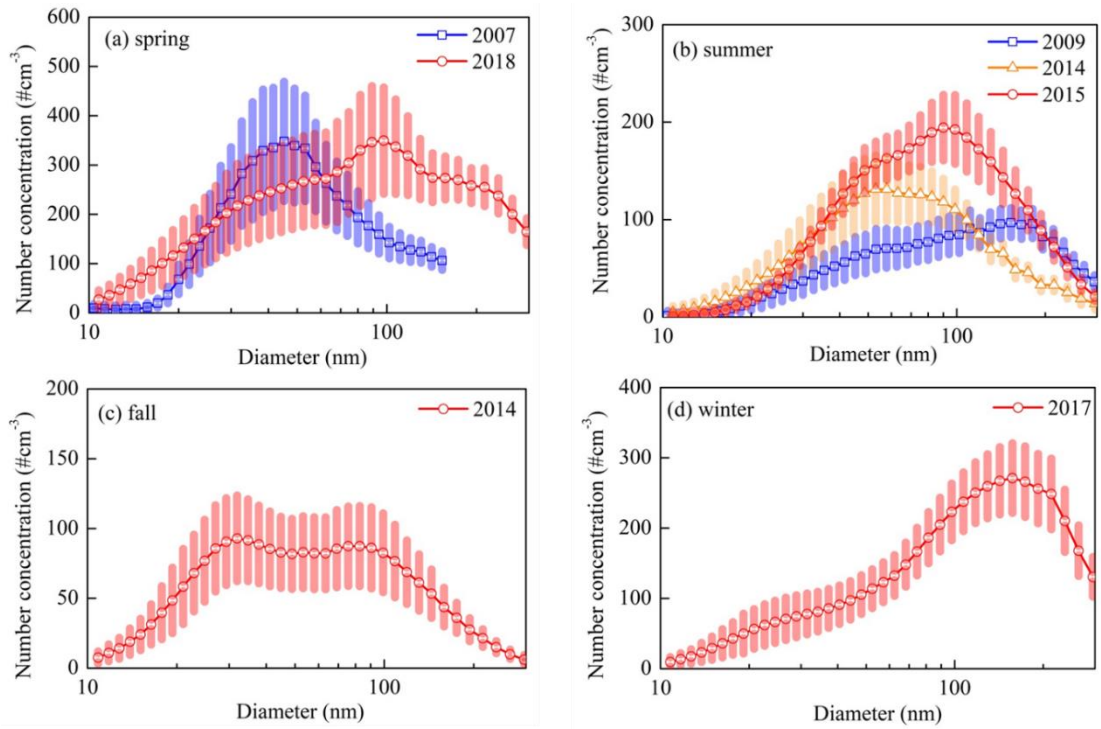

Figure R1. Particle number size distribution on non-NPF days in each campaign (shaded areas are quarter of the standard deviations).

2. Minimize, test for, and quantify campaign-specific instrument drift:

Achieving consistency in PNSD in long-term measurements is difficult. And it is not sufficient to state that each individual campaign had sufficient quality assurance, referring the reader to the campaign specific papers. There needs to be a presentation of data and discussion of how comparable the instrument responses are from campaign to campaign. What steps were taken to make sure instruments were not drifting. Aging of components can cause variation in flows, sizing accuracy, counting accuracy, particle losses, CPC supersaturations, and in the effective lower size limit of the instrumentation of the particle number spectrometer system. The detection efficiency as a function of size at the lower range of the instrument (5-25 nm), at the upper range of the mobility analyzer, at the lower end of the optical particle devices, and at the upper end of the optical particle analyzer – these are all difficult to maintain at stable levels over long periods of time. The total particle counts, height of the size distribution function, sensitivity at the lower and upper ranges of size distributions – these vary from year to year and require careful intercomparison, quality assurance, and maintenance procedures to deal with. See for example the results of intercomparison studies (Pfeifer, Müller et al. 2016) and papers focusing on quality assurance, calibration, and harmonization (Pitz, Birmili et al. 2008, Wiedensohler, Birmili et al. 2012, Wiedensohler, Wiesner et al. 2018, Gaie-Levrel, Bau et al. 2020). Comparison to other

instruments for total particle counts, size distribution functions in overlapping regions, checks with monodisperse particles are some of the techniques that can be used to establish more confidence and quantify campaign-to-campaign comparability.

Consistency in inlet dimensions, inversion algorithms (including multiple charge correction), use of impactors to manage multiple charge issues, corrections for inlet transmission efficiency, – these can all be issues in campaign-to-campaign comparability. They need to be discussed.

While being able to reproduce time-resolved PM2.5 measurements from the WPS size distribution is not sufficient to show accuracy in the nucleation and Aitken ranges – it is probably necessary. At least showing consistency from campaign to campaign in the volume of particles measured by the WPS and the mass of particles by time resolved mass measurements can help to demonstrate stability in instrumentation and data processing algorithms.

The fact that the authors are using an instrument with nominal lower cutoff of 5 nm, but discarding data between 5-10 nm indicates that there may be a problem with sensitivity at the lower size limit, or (more likely) variability in the sensitivity at the lower size limit. There is further evidence in Figures 1 and S6 – of a problem. In all the bursts shown save one, the particle size distribution function slopes down from a peak at about 13 nm to a lower value at 10 nm. If the instrument is biased low in the 10-13 nm range, then the statistics developed in the work will also be biased. If that bias varies from campaign to campaign, then that creates additional interpretation difficulties.

At line 180, it is implied that at times the WPS was collocated with instruments with lower limit of 3 nm. Therefore, the actual performance in the 5-15 nm range could (and should) be determined though comparison to such collocated instruments.

Response: Honestly, we rely on the instrument vendor on instrument maintenance and calibration every 1-2 years. Except the problem at size bins around 213 nm sometimes occurring in 2017 and 2018, the measured size distributions were reasonably consistent as mentioned above. We excluded the concentrations of particles below 10 nm for analysis in order to keep the lower limit of PNSD consistent in seven campaigns (lines 110-113 in revision). More details are presented below.

In revision, lines 118-127, we have added: "The WPS instrument was calibrated and/or repaired every 1-2 years by its vendor. The regular maintenance allowed the WPS to perform well, based on the recent comparison results of the WPS and a new scanning mobility particle sizer (SMPS, Grimm) in the summer of 2020, as shown in Fig. S3. The regular calibration parameters included the DMA sample/sheath flow, LPS sample/sheath flow, DMA/CPC pressure, DMA voltage, and DMA/ambient temperature. Polystyrene latex (PSL) spheres (NIST) with mean diameters of 100.7 nm and 269 nm were used for calibration. At the beginning of each campaign, the zero-points of the DMA, CPC, and LPS were checked using a purge filter at the inlet. Sometimes, the WPS operated improperly, and the data were excluded from the analysis (see the Fig. S4 for the occasional unexpected errors in three channels around 213 nm). In addition, we reproduced the $PM_{2.3}$ mass concentration from the WPS data and found that it was reasonably comparable to the measured $PM_{2.5}$, further supporting the accuracy of the WPS data. Details can

be found in Fig. S5 and the supplementary materials."

In addition, the aging of components may lower the detection efficiency of WPS. However, the increased FR and NMINP in 2017-2018 reveal that the signals of nucleation mode particles enhanced in recent years. In lines 260-263, it reads as "During the four campaigns in 2007, 2009, and 2014, the calculated apparent FR varied narrowly in each campaign and the campaign average narrowed to 0.8–1.2 cm^{-3} s^{-1}. The apparent FR increased in the three subsequent campaigns, i.e., 2.6 ± 1.3 cm^{-3} s^{-1} in 2015, 2.0 ± 1.7 cm^{-3} s^{-1} in 2017, and 3.0 ± 2.7 cm^{-3} s^{-1} in 2018." Therefore, we convince that the instrument maintenance can effectively reduce the aging impact of instrument components on observational data.

Conductive tubes (TSI 1/4 in.) were used for the WPS sampling, and the length of the tube was kept at approximately 2 m in each campaign. The SWS mode (DMA operating in the voltage-scanning mode) was selected. These have been added in lines 105-106, lines 108-109. The charge correction was calculated by the Boltzmann charge distribution, and the equation has been considered in the instrument algorithm.

The real-time $PM_{2.5}$ mass concentrations were measured in 2007, 2014, 2017 and 2018. Assuming that the particle density as 1.5 g cm^{-3}, the mobility diameter can be converted to the aerodynamic diameter with the equation: Aerodynamic diameter=Mobility diameter$\times \sqrt{1.5}$. The particle mass concentration in each size bin could be calculated according to the particle number concentration reported by WPS. The sum of the mass concentrations of particles less than 2.3 μm in aerodynamic diameter (1.9 μm in mobility diameter) was compared with the $PM_{2.5}$ mass concentration reported by TEOM 1400a (2007) or Thermo 5030 SHARP (2014-2018). The relationship of the hourly average data is shown in Figure R2.

For the 2007 data, we calculated the mass concentration of $PM_{0.18}$ from WPS and found that it has a weak correlation with $PM_{2.5}$. A slope of 0.05 indicated that the particles we observed accounted for only a minor fraction of the total mass of $PM_{2.5}$. For the two campaigns in 2014, the mass concentrations of WPS-derived $PM_{2.3}$ and SHARP measured $PM_{2.5}$ showed good correlations, with slopes of 0.69-0.76. For the 2017 and 2018 data, we removed the abnormal data in three bins around 213 nm. A good linear correlation was obtained between the two variables, but the slopes slightly increased to 0.86-0.9. Note that the calculation results depend on the adopted density of the particles. The actual particle density may deviate from the assumed value. In such cases, the sum volume (mass) may suffer from an error to some extent. The difference in the slopes may be partially related to the single value of particle density in different years, but other unknown factors cannot be excluded. Nevertheless, all of the deviations were less than 30%, and the linear correlations were generally good. However, the comparison alone cannot warrant the WPS operating properly. These have been added in the revised supplementary.

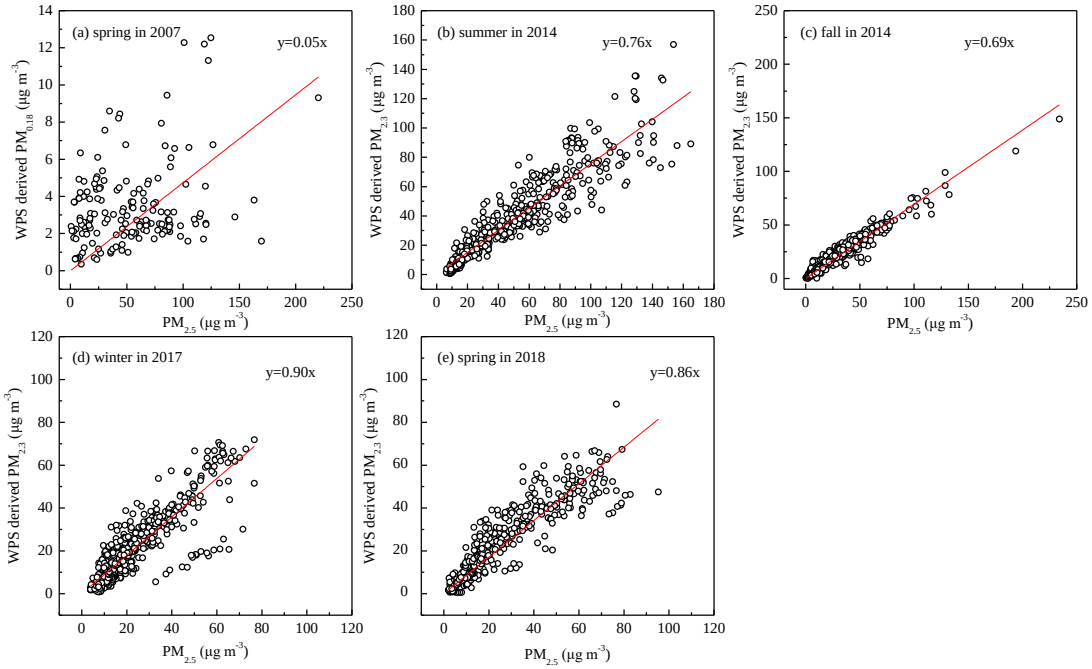

Figure R2: The relationship between $PM_{2.5}$ mass concentrations reported by TEOM 1400a (or Thermo 5030 SHARP) (x-axis) and PM mass concentrations derived from WPS (y-axis).

As we mentioned above, the detection limit of the DMA was 10 nm in 2007 and 2009, while it was 5 nm in 2014, 2015, 2017, and 2018. For consistency, only concentrations of >10 nm particles were used for the analysis. On April 7 (Fig. 1b in origin version and Fig. 1c in revised version), the initial peak at about 13 nm. That because the initial nucleation was influence by sporadic spikes, which overwhelmed the nucleation signal. In revision, lines 184-186, we added "Note that a few spikes were occasionally observed with a broader particle number size distribution during the NPF period. These spikes were excluded in the calculation of the FR, GR, D_{pg}, NMINP and CCN parameters (described in 2.2.2) because they may reflect primary particles from localized sources (Liu et al., 2014; Man et al., 2015; Zhu et al., 2017)." The revised D_{pg} as shown in Fig. 1c.

The measurements made by NAIS at Mt. Tai were reported by Lv et al. (2018). But we have no confidence on the raw NAIS data. Fortunately, we have conducted a comprehensive comparison between the WPS and a SMPS (GRIMM, Germany) at a costal site in Qingdao, China, during 2-7 July 2020. The SMPS consists of a DMA (55-U，GRIMM) and a CPC (5416，GRIMM). It covers the particle size range of 10 nm-1000 nm, and is set up to 127 channels. The time resolution of SMPS is 4 min. The two instruments of WPS and SMPS were operated side by side for intercomparison.

Figure R3 shows the comparison of particle number concentration in the range of 10-25 nm (nucleation mode) and 10-300 nm (particle size range we used for calculation in this paper) between WPS and SMPS. Particle number concentration in these two size ranges showed good linear correlations, suggesting the measurements of the two instruments are highly consistent. Furthermore, the highly correlated data indicates that the WPS is not experiencing aging problems.

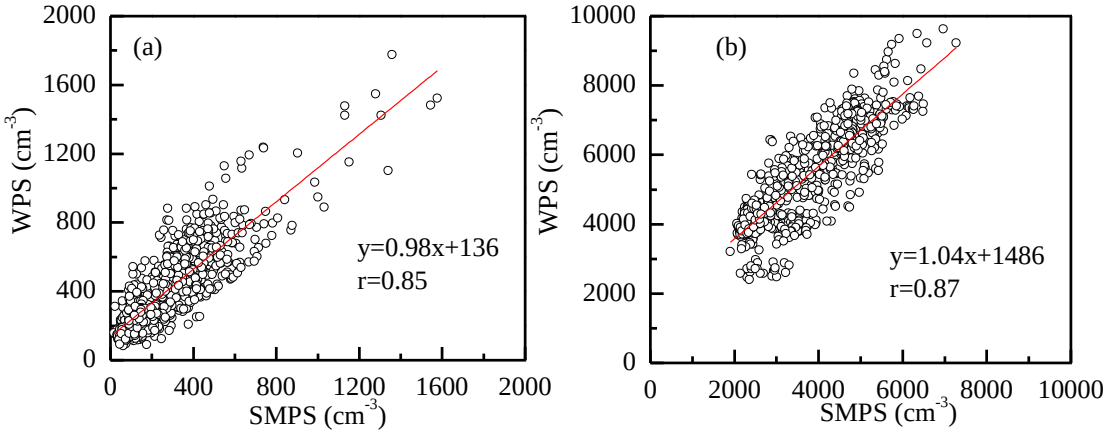

Figure R3 Comparison of particle number concentration in 10-25 nm (a) and 10-300 nm (b) between WPS and SMPS during 2-7 July 2020.

3. Consistency in subjective data interpretation/classification steps:

It is not clear which of the variables used for analysis involve human classification. Sometimes, human classification is used for PFGE types (often using how smooth the growth event is in time); human classification is used sometimes for establishing times (start of event, end of the event). The end time is described. From line 113 of manuscript, "The end time of an NPF event was defined as the time when the particle number concentrations approached the background levels observed before the NPF event. The NPF event duration was defined as the time duration between the start time and end time of an NPF event." This seems like the end of event was a subjective determination of when background was approached. Thus the end time, duration, and any rate that has the duration in the denominator may be subjective.

For subjective (human) event classifications, were the events uniformly reclassified for this paper, or were prior classifications adopted from 2007 and 2009 and mixed with new classifications done for the more recent campaigns. See (Dal Maso, Kulmala et al. 2005) for best practices on human classification.

Response: In revision, lines 152-156, we have added the details when classifying NPF events: "In this study, particles with diameters smaller than 25 nm were defined as nucleation mode particles (Kulmala et al., 2012). Following the criteria proposed by Dal Maso et al. (2005) and Kulmala et al. (2012), three features had to be met for an event to qualify as NPF: 1) a distinctly new nucleation mode particles must appear in the size distribution; 2) the new mode should prevail over a time span of hours; and 3) the new mode should show signs of growth. All three features are required for a day (00:00-23:59 LT) to be classified as an NPF day. Otherwise, the day is classified as a non-NPF day."

The definition of "NPF duration" has been added in lines 157-164: "The initial time of an NPF event was defined as when new nucleation mode particles started to be observed (e.g., t_0 in Fig. 1b, d). The end time of an NPF event was defined as the new particle signal dropping to a negligible level and the total particle number concentrations approaching the background levels

before the NPF event. In cases with the invasion of other plumes, the end time was determined to be when the new particle signals were suddenly overwhelmed by plumes and could no longer be identified (e.g., the end times in Fig. 1b, d). The NPF event duration was defined as the time duration between the initial time and end time of an NPF event. Note that the detection limit of WPS was 10 nm, but the particles were nucleated at critical cluster sizes of approximately 1-1.5 nm. Therefore, the NPF actually occurred at some time prior to our observation, and the actual duration should be longer than our calculation."

Followed the definition above, we classified the NPF event uniformly during the seven campaigns, i.e., from 2007 to 2018. In addition, the schematic diagram of t_0 and end time, as well as other NPF parameters such as NMINP and ΔN_{CCN} has been added in Fig. 1 (as shown in Figure R4). Moreover, Figure R4b also shows that the choice of t_0 may lead to underestimation of ΔN_{CCN} to some extent in the presence of spatial-temporal heterogeneity of pre-existing particles with diameters larger than 50 nm. In these cases, the mean value of N_{CCN} in the percentiles smaller than 5^{th} during the whole NPF event may be more accurate representing the background (see the grey dashed line in Figure R4 b). However, this method may also introduce more subjective factors and therefore was not adopted in this study. These have been added in lines 214-218.

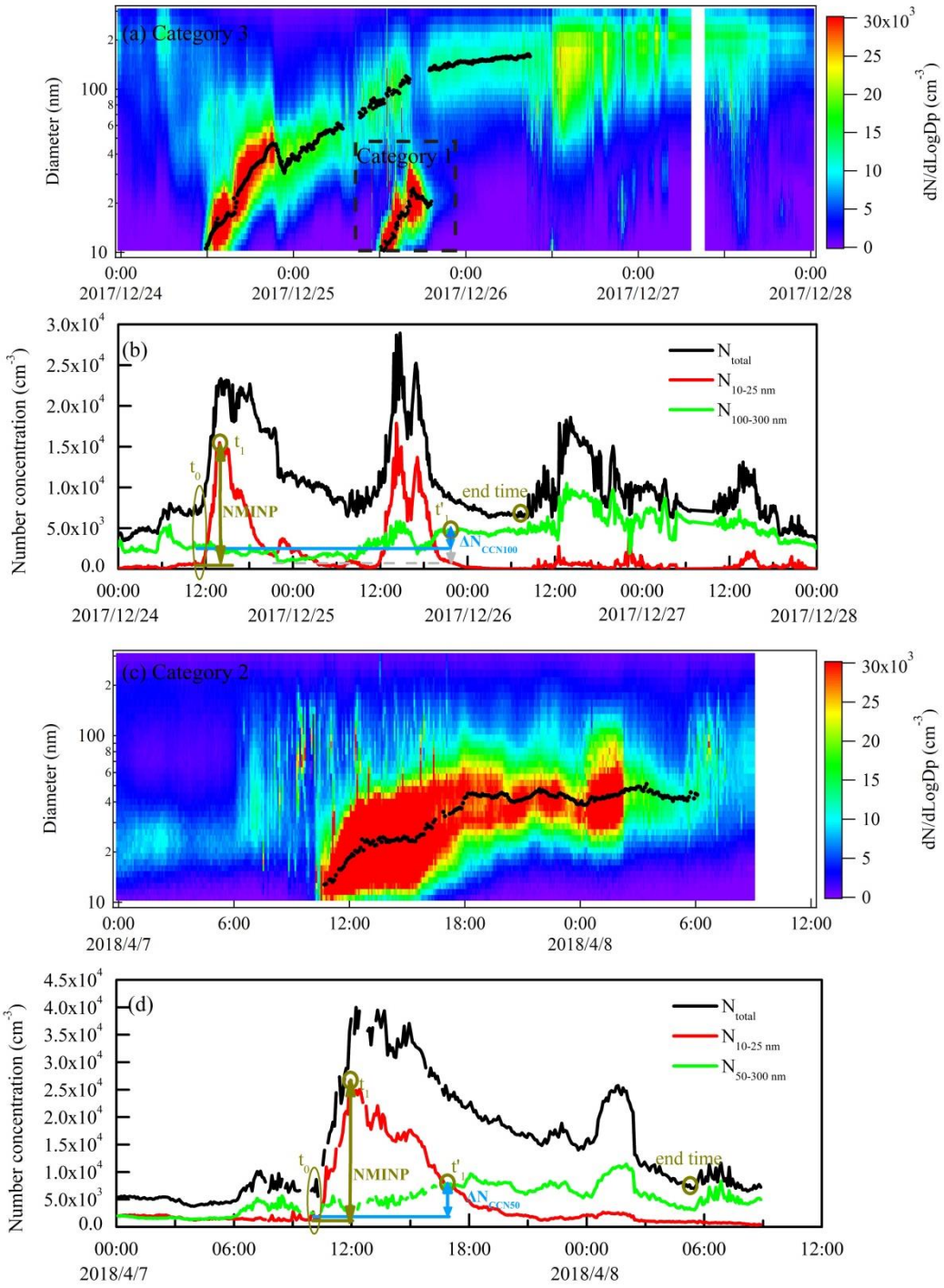

Figure R4 Examples of NPF events in three categories. Black dots in the figures are the fitted D_{pg}. (a) Category 1 on December 25, 2017, in which D_{pgmax} was 24 nm (<50 nm), and Category 3 on December 24, 2017, in which D_{pgmax} grew to 163 nm (>80 nm); (c) Category 2 on April 7, 2018, in which D_{pgmax} grew to 53 nm (50–80 nm). (b, d) Schematic diagram of t_0, t_1, t'_1, NMINP and $\Delta N_{CCN100}/\Delta N_{CCN50}$ on December 24, 2017 and April 7, 2018 NPF events (a few spikes have been removed in Figure d).

4. Statistical methods appropriate to analysis of combined seasonal and interannual variability

Statistical procedures for evaluating trends in seasonally varying time series need to be followed in order to state claims that trends exist. These can be found in a number of textbooks, papers, and government reports. See for example Statistical Methods for Environmental Pollution Monitoring by Gilbert https://www.osti.gov/servlets/purl/7037501/. And (Asmi, Coen et al. 2013, Collaud Coen, Andrews et al. 2013, Squizzato, Masiol et al. 2019). Many other good models for seasonally adjusted trend detection can be found in the O3, NOx, PM2.5, and hydrology/climatology literature. Squizzato et al. (2019) for example have the statistical procedures necessary to detect turning points (see line 236 where manuscript discusses turning points)

See for example line 290 "the CS still increased in 2018 compared with that in 2007." That implies annual average condensational sink increased, and this is a season or month specific result – and it is not clear there is enough statistical confidence to state this. Many other locations in the paper have broad statements about PFGE behavior in one year vs. another, or imply a long term trend where it has not really been shown.

Interpretation of PFGE data from this site seems more complicated than most, because of two issues: (1) it is sometimes influenced by boundary layer and other times by free troposphere; (2) very long PFGE events (see for example Figure 1a, where a 3-d long event is shown) are being compared with shorter (midday + afternoon) growth events. See Figure 7 which has events ranging from 3-h duration to 85-h duration. The flow patterns and chemistry required to sustain a 3-h event and an 80+ h event are likely very different, and would require more thoughtful comparison metrics than used in the paper.

The paper acknowledges this difficulty in interpretation (line 295) but more needs to be done than just acknowledge the difficulty. See analysis papers from PFGE studies at other high altitude sites. They do attempt to determine the degree of FT influence and the impact of polluted boundary layer air. And there are many papers that factor in air mass characteristics and/or back trajectory in analysis of PFGE.

See for example Figure 1a where on 25-Dec 2017 there were simultaneously occurring a short PFGE (category 1) and evolution of the category 3 event that started on 24-Dec 2017. This raises a number of questions on how such a dataset can be analyzed to determine trends.

How much of the variability in data is that some campaigns had more free tropospheric influence and others have less. How much of the conclusions of the paper are driven by switches (during PFGE) in air mass influence to/from FT influence. In other words, PFGE events that have their evolution dynamics controlled by airflows, and not by chemistry – hence the authors observed lack of influence or counterintuitive effects of SO2.

As for statistical procedures, I think it would be much more appropriate to put 95% confidence intervals on means rather than standard deviations on the plots. (Most figures have standard deviations)

Some of the variables appear to NOT be normally distributed (see figure S4) and thus use of statistical tests designed for normally distributed data are inappropriate.

Another weakness of the approaches used are that changes in boundary layer height are not accounted for. This weakness cannot really be addressed without additional measurements, but it

should be noted.

Response: We acknowledge that the technical term "trend" is misleading in the origin manuscript. It has been removed in the revision. The "turn point" was inappropriate and we removed this in revision. We are also honest to say that we cannot understand those comments on other statistical issues.

Lines 370-373 (line 290 in origin version) has been revised as "Note that the campaign average $PM_{2.5}$ mass concentration in 2018 indeed decreased. The decrease was apparently determined by the decrease in >153 nm particles, since no significant difference existed in the calculated CS based on <153 nm particles between 2007 ($0.32\pm0.19\times10^{-2}$ s^{-1}) and 2018 ($0.40\pm0.15\times10^{-2}$ s^{-1})." We didn't imply the annual trend of CS or other variables, we have checked the full text and revise the ambiguous statements.

Here we comprehensively analyze four cases of NPF events in different categories (category 1 events on 5 April 2007 and 6 April 2018, category 2 event on 8 April 2018), and category 3 event on 23 April 2007) in 2007 and 2018. The meteorological parameters, gases pollutants, PM2.5 mass concentrations and planetary boundary layer height (PBLH, download from https://goldsmr4.gesdisc.eosdis.nasa.gov/data/MERRA2/M2T1NXFLX.5.12.4/) were showed in figure R5 and R6. PBLH shows obvious diurnal variations, and the maximum value are 4110 m, 3000 m, 2316 m, and 2224 m on 6 April 2018, 7 April 2018, 5 April 2007, and 23 April 2007. There was no significant difference in the evolution of PBLH among the three categories. In revised Fig. S12, we also plotted the PBLH in three types of NPF events. In lines 425-427, we added "In addition, the changed boundary layer height had no detectable influence on D_{pgmax} as shown in Fig. S12. However, the change in the late afternoon may largely decrease the observed number concentrations of grown new particles." We argued that PFGE events were controlled by chemistry, since the changes of airflow always associate with the changes of air pollutant, which directly influence NPF as mentioned in the response to the first comment.

As reported in numerous literatures, the growth of newly formed particles is mainly attributed to sulfuric acid, ammonium nitrate, and secondary organic compounds (Wiedensohler et al., 2009; Riipinen et al., 2011; Zhang et al., 2012; Ehn et al., 2014; Man et al., 2015; Wang et al., 2015; Burkart et al., 2017; Lee et al., 2019; Wang et al., 2020b). We therefore explore their respective contributions as follows. First, we calculated the contribution of sulfuric acid to the growth based on the observed mixing ratio of SO_2 and equations (5)-(6) in section 2.2.3. Second, we examined whether NH_4NO_3 freshly formed in $PM_{2.5}$ during the particle growth period. In case of no NH_4NO_3 formation, its contribution would not be expected. This is because an even higher product of $HNO_3gas*NH_3gas$ is required to overcome the kelvin effect and form NH_4NO_3 in nucleation mode and Aitken mode particles. Thus, the growth unexplained by sulfuric acid should be mainly contributed by organics. In case of NH_4NO_3 formation, we considered the net increase in NH_4NO_3 may contribute to the particle growth, even though the ratios of increased NH_4NO_3 in $PM_{2.5}$ may not be the same as the ratios in nucleation mode and Aitken mode particles.

On 6 April 2018 (category 1), the NPF event was first observed at 09:10. D_{pg} was fitted as 13 nm at 09:45, and continuous grow to 30 nm at 18:10. Then both of the particle number

concentration and particle diameter decreased, and the plume overwhelm the new particle signal at 6:00 on 7 April. During the NPF period, sulfuric acid was estimated to contribute about 16% to particle growth. The mass concentration of nitrate in $PM_{2.5}$ was less than 1.0 μg m^{-3}, implying that fresh NH_4NO_3 formation did not occur. Thus, the growth unexplained should be mainly contributed by organic matter.

On 7 April 2018 (category 2), D_{pg} increased from 13 nm at 10:00 to 43 nm at 18:00, then D_{pg} fluctuate at 41 nm-52 nm in the following 10 hours. Sulfuric acid was estimated to contribute about 11% to particle growth. The mass concentration of nitrate in $PM_{2.5}$ continuously increased from 0.8 μg m^{-3} at 10:00 to 2.7 μg m^{-3} at 20:00, then decreased to 2 μg m^{-3} at 4:00 on 8 April 2018. Formation of ammonium nitrate seems to contribute to the growth of new particles in this case.

Similarly, on 23 April 2007 (category 3), sulfuric acid was estimated to contribute about 23% to particle growth. The mass concentration of nitrate in $PM_{2.5}$ increased from 1 μg m^{-3} to 10 μg m^{-3} during the particle growth period, indicating its important role in the particle growth. On the contrary, the mass concentration of nitrate and sulfate decreased during the NPF period on 5 April 2007 (category 1), and new particles didn't grow to the larger size.

We summarized the mass concentration of SO_4^{2-}, NO_3^-, NH_4^+ and OC during the formation and growth period of NPF events in 2007 and 2018 campaigns (added in revised Table 2). During the growth periods, the contribution of H_2SO_4 vapor to particle growth decreased from 36% in 2007 to 11% in 2018. The mass concentration of nitrate in $PM_{2.5}$ was 7.4 ± 4.8 μg m^{-3} in 2007 during the new particle growth period, and it slightly decreased to 6.7± 5.5 μg m^{-3} in 2018. In addition, OC in $PM_{2.5}$ was lower in 2018 (5.5 ± 2.0 μg m^{-3}) than in 2007 (6.1 ± 3.0 μg m^{-3}). In 2018 campaign, the reduced H_2SO_4 vapor, nitrate and OC formation may lead to the decrease in the growth probability of new particles. However, large uncertainties still exist because of a lack of data on the chemical composition of these smaller particles. These have been added in section 4.2.

Two sets of data in Fig. S4 (Fig. S10 in revision) are not linearly correlated, and we removed the fitting equations and changed the figure to scatter plots.

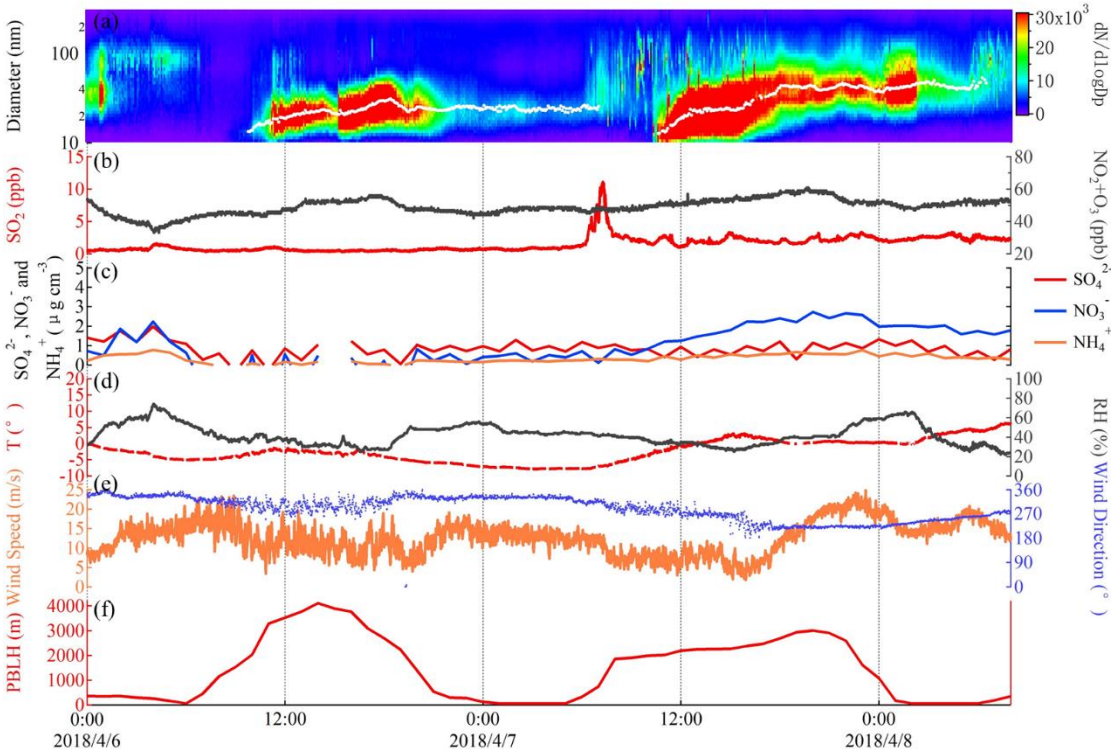

Figure R5 Time series of NPF events on 6 April 2018 and 7 April 2018: (a) contour plot of particle number size distribution using WPS data; (b) SO2 and NO2+O3; (c) mass concentration of SO42-, NO3- and NH4+ in PM2.5; (d) temperature (T) and relative humidity (RH); (e) wind speed and wind direction; (f) Planetary boundary layer height (PBLH).

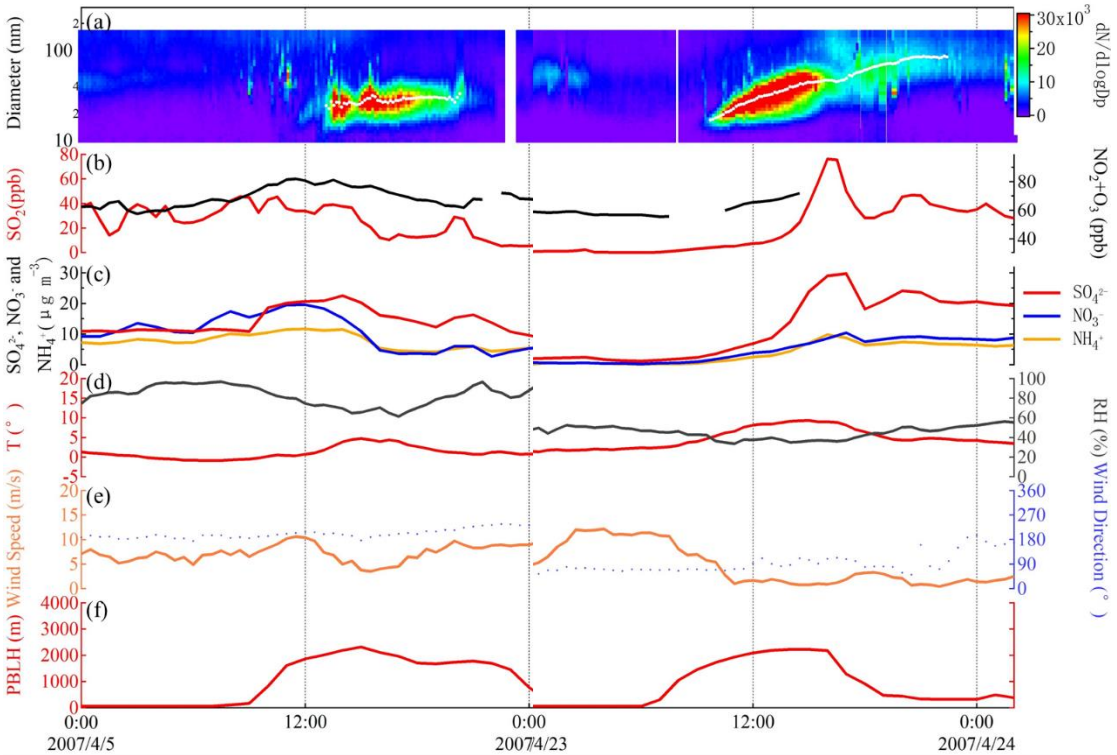

Figure R6 Time series of NPF events on 5 April 2007 and 23 April 2007: (a) contour plot of

particle number size distribution using WPS data; (b) SO2 and NO2+O3; (c) mass concentration of SO42-, NO3- and NH4+ in PM2.5; (d) temperature (T) and relative humidity (RH); (e) wind speed and wind direction; (f) Planetary boundary layer height (PBLH).

Other issues:

5. The abstract overstates the conclusions of the work. The conclusions have significant caveats, are based on limited number of sampled days, but the abstract makes it seem like the trends are well established, statistically significant, and based on a complete multi-year time series.

Response: Thanks. We have removed the "trend" in revision and revised the abstract.

6. There are a number problems with Figure 6. It is not appropriate to grey out datasets that are not correlated. Data are data, and data points should not be deemphasized visually just because they do not fit a linear correlation. The datasets should be clearly labeled so that each symbol type can be connected back to its underlying study and land cover type. Having a linear correlation shown and then a change in the tick mark spacing is not a fair way of graphing in my opinion. The size ranges in question should be included in the axis labels and/or the caption. I believe this is the formation rate at 10 nm, and the NMINP at 10-25 nm? Is that consistent for all the datasets? If not, then I don't think this is a fair plot to put in. I don't think having regression equations and correlation coefficients on graphs is effective or appropriate (see additional comments on this later).

Response: Thanks. We have changed the grey markers to black markers, as shown in Figure R7. In this study at Mt. Tai station, all of the FR and NMINP are linearly correlated, and FRs were less than 15 $cm^{-3}s^{-1}$ (blue markers in Figure R7). Therefore, the linear relationship was the key point we would like to address, and we change the tick mark space when FR larger than 20 $cm^{-3}s^{-1}$ in order to emphasize our data at Mt. Tai.

We confirmed that the FR and NMINP were calculated based on 10-25 nm particles in all cases in this figure.

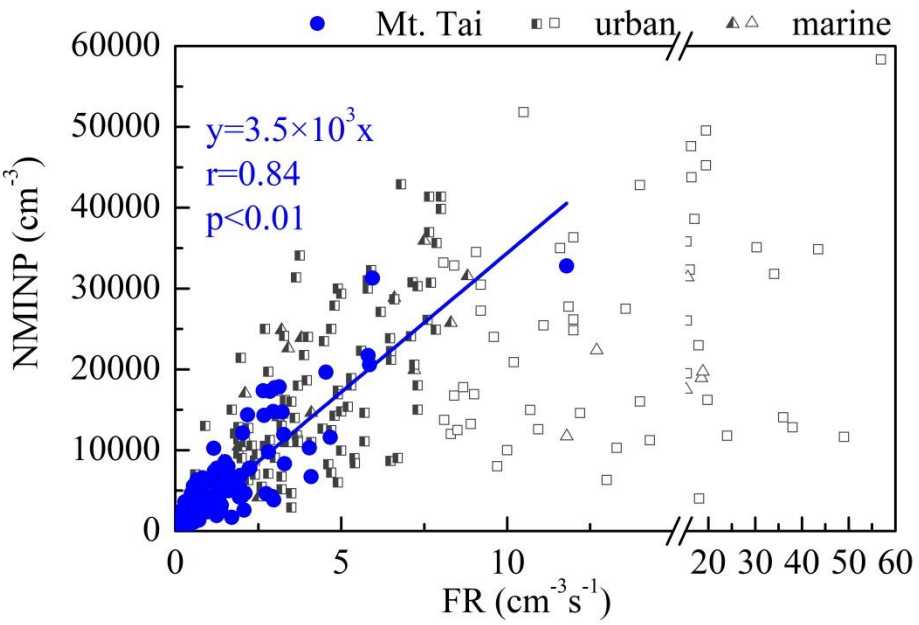

Figure R7 Relationship between the FR and NMINP in 106 cases of NPF events at Mt. Tai in this study and in urban and marine atmospheres in previous studies (Man et al., 2015; Zhu et al., 2017, 2019; Ma et al., 2020). Semi-solid markers can be fitted linearly in previous studies. Open markers show poor correlations.

7. If a p-value appears in a figure or in the paper, then the statistical test needs to be discussed. What are the null and alternative hypothesis. And why is each hypothesis test implied by each p value important, scientifically interesting, novel, or useful?

Response: The significance of P value is commonly required for any correlation or regression analysis and has been added in revision. We cannot understand what the reviewer wanted to comment. We are sorry for this.

8. If a regression equation (e.g., y=12.5x+5.6) appears in a figure or in the paper, then its use – either for scientific or engineering purposes – needs to be discussed. The paper has 9 regression equations in it. Are they of any use?

Response: Yes, the equation has its implication. For example, in type A, the D_{pgmax} and GR can be fitted by the equation: D_{pgmax} = 11.0×GR+8.2 with a moderate good *r*. Based on the obtained equation, newly formed particles appear to grow beyond 50 nm only when the GR exceeds 3.8 nm h^{-1} in Type A. In addition, based on the regression equation between the duration and D_{pgmax} obtained in 2007–2015 and 2017–2018, newly formed particles could grow beyond 50 nm only when the NPF duration exceeded 9.9 h in 2007–2015, but the duration in 2017-2018 had to exceed 27.8 h. In type B, following the regression equation of D_{pgmax} against GR, newly formed particles

in Type B could grow beyond 50 nm only when the GR exceeded 5.8 nm h^{-1}. These have been added in lines 397-399, lines 400-402, lines 418-420.

9. I believe all r values can be deleted from the paper without any loss.

Response: Correlation coefficient is a statistical concept, which helps in establishing a relation between predicted and actual values obtained in a statistical experiment. The calculated value of the correlation coefficient explains the exactness between the predicted and actual values. The r values are used to measure the degree of correlation between two variables. A high r value (close to 1) means that the variables are highly correlated, and the fitted equation has its physical meaning. A small r value (close to 0) means the two variables are irrelevant, and the fitted equation is meaningless.

10. Is the size range covered sufficient for calculating the condensational sink? Or stated differently, how much of the condensational sink is being missed by focusing on 10 to 150 or 250 nm.

Response: We recalculated the CS in different size ranges, i.e., 10 nm-2.5 μm, 10 nm-300 nm and 10 nm-153 nm of particles in the campaign of 2018. The average CS values were $0.80\pm0.37\times10^{-2}$ s^{-1}, $0.75\pm0.34\times10^{-2}$ s^{-1}, and $0.40\pm0.15\times10^{-2}$ s^{-1} for the three ranges of particles, respectively. The CS calculated by the use of particles in the range of 10 nm-300 nm accounted for 94% of those in the range of 10 nm-2.5 μm. Hence, the size range of 10-300 nm is sufficiently accuracy to estimate the condensational sink for comparing among different campaigns. However, the CS calculated by the use of particles in the range of 10 nm-153 nm accounted for only half of that in the range of 10 nm-2.5 μm. Thus, the CS calculated by the use of particles in the range of 10 nm-153 nm in 2018 was also used to compare with that in 2007. These have been added in lines 170-176, lines 370-373 and the supplementary materials.

11. Line 138 "can be calculated" or was calculated?

Response: It should be "was calculated".

12. Are variables that are sensitive to the upper size limit (CCN concentrations that are based on the number of particles greater than size X, condensation sink) consistent given the change in the upper size limit shown in Figure S3, from campaign to campaign.

Response: In this study, 10–300 nm particles were used to calculate ΔN_{CCN} in all campaigns except for that in spring 2007. In the particular year, the data of >153 nm particles were missing. Alternatively, the data of 10–153 nm particles were used for the calculations. The lack of 153-300 nm particles may have led to the smaller ΔN_{CCN} in 2007. For example, Figure R8 shows the PNSD at 19:30-20:30 on April 23, 2007, when we calculated the CCN number concentrations, i.e., $N_{CCN}(t'_1)$. On that day, the maximum size of geometric median diameter of the grown new particles (D_{pgmax}) was the largest (89 nm) during the spring campaign in 2007. The lognormal fitted curve showed that approximately 15% of the area was missing to gain a complete accumulation mode, suggesting that $N_{CCN}(t'_1)$ was underestimated by ~15%. In other events, the D_{pgmax} was smaller, and the missing areas in the PNSD curve caused even smaller underestimation. Thus, it is safe to say that the lack of data for >153 nm particles had a negligible effect on the calculated ΔN_{CCN} in 2007. These have been added in lines 219-222 and the supplementary materials.

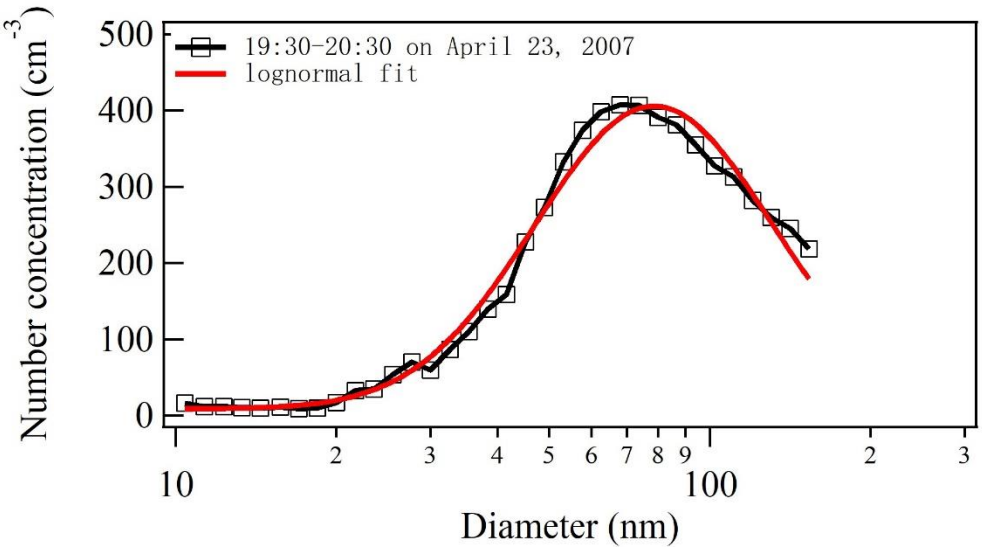

Figure R8 PNSD during 19:30-20:30 on April 23, 2007, i.e., $N_{CCN}(t'_1)$.

13. Line 282 – climate change typically requires 30-y averaging. Interannual variability may be much more likely at the time scales studied here.

Response: It has been revised to "Previous studies have reported that the BVOC emissions over the NCP have substantially increased in the last decade because of rapid afforestation and accelerating global warming."

14. Line 293 – "data size was small" is vague. A more detailed description of what aspects of the dataset are too small is needed.

Response: It has been revised to "the data were obtained in seven independent campaigns, each

lasting in 18~71 days, and the data size did not allow us to extend the conclusion to all the years from 2007 to 2018."

15. Line 294 – there are two issues: spatial representativeness, and sparsity of the record in time. In my opinion these create two different problems for the work. "the data size was small, and we should be cautious in extending the conclusion to a large spatiotemporal scale"

Response: It has been revised to "However, uncertainties still exist, e.g., 1) the data were obtained in seven independent campaigns, each lasting in 18~71 days, and the data size did not allow us to extend the conclusion to all the years from 2007 to 2018; 2) the observations were conducted only at one site, alternating between the boundary layer and the free troposphere, and the generality of the conclusions on NPF events needs to be examined at more sites.".

16. Line 299 – this shows the authors are thinking of these events as perfect Lagrangian experiments, where sampling at the mountain site is equivalent to sampling along a 0-D Lagrangian air mass trajectory. Vertical and horizontal mixing are not accounted for in this conceptual model. And the possibility that back trajectories evolve over the course of the PFGE is neglected. In reality, as the event evolves, winds will bring air with a variety of histories (chemical, emissions, radiation, accumulation mode particles, interaction with precipitation and clouds, etc.). The survival probabilities over 100% (Figure 4) are likely a symptom of the fact that reality has complex flows and spatial heterogeneity and does not fit the idealized box model concept.

Response: We agree that the vertical and horizontal mixing play an important role in the observed NPF events. If the ambient nucleation occurs aloft and newly formed particles mixes down to the height to be observed, the observed FR may be determined mainly by the downward moving rate of newly formed particles rather than the true formation rate of newly formed particles. Thus, we change "formation rate" to "apparent formation rate" in revision.

However, the growth rate and D_{pgmax} of newly formed particles were determined by concentrations and cumulative amounts of the condensed vapors, respectively. The condensed vapors are commonly believed to be generated from chemical reactions in air masses regardless of the moving rates of air masses in vertical and horizontal directions.

It does not make sense to calculate the SP beyond 100% because of highly spatial-heterogeneity of NPF in those particular events. In the revision, we added "Note that the spatial-temporal heterogeneity during NPF events may result in high SPs. If the observed ΔN_{CCN} exceeded NMINP and the calculated SPs exceeded 100%, suggesting equation (3) was not applicable in these cases, and SP was therefore not calculated."

17. Figure 7 is of low resolution. Difficult to see some of the symbols, and symbols are of different

sizes in different plots.

Response: corrected.

18. The discussions of biogenic and total VOCs throughout the paper are problematic. What species are these? How were they measured? Were the measurements collocated with the PFGE measurements and matched in time? The amount of oxidation needed to grow from 3 to 10 nm or 10 to 20 nm, is quite small, so making broad generalizations about seginficant changes in entire classes of VOCs or in specific compounds, and then connecting them to PFGE is not scientifically valid.

Response: The total VOCs in the June 2006 campaign was cited from Mao et al. (2009), since no data from the spring 2007 campaign were available. As many as 52 VOCs (C_4–C_{12}) were measured. The analyses method and the species list of VOCs can be found in Mao et al. (2009). In the spring 2018 campaign, a total of 30 whole-air samples were collected on 9 days. The concentrations of VOCs were then quantified by gas chromatography (GC) separation followed by flame ionization detection (FID), mass spectrometry detection (MSD), and electron capture detection (ECD) at the laboratory of the University of California at Irvine (UCI). As many as 75 VOCs (C_2–C_{10}) non-methane hydrocarbons (NMHCs) were measured. The analyses method can be found in Chen et al. (2020). We acknowledge that the analytical methods were different in the two campaigns, and the difference in the VOCs has been added in revision, lines 365-366.

In addition, a recent study reported that China has experienced rapid afforestation, with provincial forest areas increasing by between 0.04 million and 0.44 million hectares per year over the past 10 to 15 years, leading to a large increase in the CO_2 sink based on long-term observations over large spatial scales (Wang et a., 2020a). BVOC emissions in China are reasonably expected to greatly increase over the past 15 years. This was highly consistent with the difference between the VOCs concentration at Mt. Tai in 2006 and 2018. However, a large knowledge gap between the increase in BVOC emissions and the increase in nucleating organics still exists because of a lack of studies. These have been added in revision, lines 67-71 and lines 367-369.

19. Rather than making the data available "on request", the data should be publicly posted in machine readable formats at the time of publication in order to allow replication.

Response: Thanks, we have provided the website to access the datasets in revision.

Reference:

Birmili, W. and A. Wiedensohler (2000). "New particle formation in the continental boundary layer: Meteorological and gas phase parameter influence." Geophysical Research Letters 27(20): 3325-3328.

Burkart, J., Hodshire, A. L., Mungall, E. L., Pierce, J. R., Collins, D.B., Ladino, L. A., Lee, A. K., Irish, V., Wentzell, J. J., Liggio, J., and Papakyriakou, T. (2017). Organic condensation and particle growth to CCN sizes in the summertime marine Arctic is driven by materials more semivolatile than at continental sites, Geophys. Res. Lett., 44, 10725–10734.

Dal Maso, M., M. Kulmala, I. Riipinen, R. Wagner, T. Hussein, P. P. Aalto and K. E. J. Lehtinen (2005). "Formation and growth of fresh atmospheric aerosols: eight years of aerosol size distribution data from SMEAR II, Hyytiala, Finland." Boreal Environment Research 10(5): 323-336.

Ehn, M., Thornton, J.A., Kleist, E., Sipilä, M., Junninen, H., Pullinen, I., Springer, M., Rubach, F., Tillmann, R., Lee, B., Lopez-Hilfiker, F., Andres, S., Acir, I., Rissanen, M., Jokinen, T., Schobesberger, S., Kangasluoma, J., Kontkanen, J., Nieminen, T., Kurtén, T., Nielsen, L.B., Jørgensen, S., Kjaergaard, H.G., Canagaratna, M., Maso, M.D., Berndt, T., Petäjä, T., Wahner, A., Kerminen, V., Kulmala, M., Worsnop, D.R., Wildt, J., and Mentel, T.F. (2014). A large source of low-volatility secondary organic aerosol, Nature, 506.

Gaie-Levrel, F., S. Bau, L. Bregonzio-Rozier, R. Payet, S. Artous, S. Jacquinot, A. Guiot, F. X. Ouf, S. Bourrous, A. Marpillat, C. Foulquier, G. Smith, V. Crenn and N. Feltin (2020). "An intercomparison exercise of good laboratory practices for nano-aerosol size measurements by mobility spectrometers." Journal of Nanoparticle Research 22(5): 13.

Kulmala, M., Petäjä, T., Nieminen, T., Sipilä, M., Manninen, H. E., Lehtipalo, K., Dao Maso, M., Aalto, P. P., Junninen, H., Paasonen, P., Riipinen, I., Lehtinen, K. E. J., Laaksonen, A., and Kerminen, V-M.(2012). Measurement of the nucleation of atmospheric aerosol particles, Nat. Protoc., 7, 1651–1667.

Lee, S., Gordon, H., Yu, H., Lehtipalo, K., Haley, R., Li, Y., and Zhang, R. (2019). New Particle Formation in the Atmosphere: From Molecular Clusters to Global Climate, J. Geophys. Res. Atmos., 124, 7098-7146.

Ma, L., Zhu, Y., Zheng, M., Sun, Y., Huang, L., Liu, X., Gao, Y., Shen, Y., Gao, H., and Yao, X. (2020). Investigating three patterns of new particles growing to cloud condensation nuclei size in Beijing's urban atmosphere, Atmos. Chem. Phys. Diss.

Mao, T., Wang, Y., Xu, H., Jiang, J., Wu, F., and Xu, X. (2009). A study of the atmospheric VOCs of Mount Tai in June 2006, Atoms. Envrion., 43, 2503-2508.

Man, H., Zhu, Y., Ji, F., Yao, X., Lau, N.T., Li, Y., Lee, B.P., and Chan, C.K. (2015). Comparison of Daytime and Nighttime New Particle Growth at the HKUST Supersite in Hong Kong, Environ. Sci. Technol., 49, 7170-7178.

Pfeifer, S., T. Müller, K. Weinhold, N. Zikova, S. Martins dos Santos, A. Marinoni, O. F. Bischof, C. Kykal, L. Ries, F. Meinhardt, P. Aalto, N. Mihalopoulos and A. Wiedensohler (2016). "Intercomparison of 15 aerodynamic particle size spectrometers (APS 3321): uncertainties in

particle sizing and number size distribution." Atmospheric Measurement Techniques 9(4): 1545-1551.

Pitz, M.,W. Birmili, O. Schmid, A. Peters, H. E. Wichmann and J. Cyrys (2008). "Quality control and quality assurance for particle size distribution measurements at an urban monitoring station in Augsburg, Germany." Journal of Environmental Monitoring 10(9): 1017-1024.

Riipinen, I., Pierce, J. R., Yli-Juuti, T., Nieminen, T., Häkkinen, S., Ehn, M., Junninen, H., Lehtipalo, K., Petäjä, T., Slowik, J., Chang, R., Shantz, N. C., Abbatt, J., Leaitch, W. R., Kerminen, V.-M., Worsnop, D. R., Pandis, S. N., Donahue, N. M., and Kulmala, M. (2011). Organic condensation: a vital link connecting aerosol formation to cloud condensation nuclei (CCN) concentrations, Atmos. Chem. Phys., 11, 3865–3878.

Wang, Z.B., Hu, M., Pei, X.Y., Zhang, R.Y., Paasonen, P., Zheng, J., Yue, D.L., Wu, Z.J., Boy, M., and Wiedensohler, A. (2015). Connection of organics to atmospheric new particle formation and growth at an urban site of Beijing, Atmos. Environ., 103, 7-17.

Wang, J., Feng, L., Palmer, P. I., Liu, Y., Fang, S., Bösch, H., O'Dell, C. W., Tang, X., Yang, D., Liu, L., and Xia, C. Z. Large Chinese land carbon sink estimated from atmospheric carbon dioxide data, Nature, 586, 720-723, https://doi.org/10.1038/s41586-020-2849-9, 2020a.

Wang, M., Kong, W., Marten, R., He, X., Chen, D., Pfeifer, J., Heitto, A., Kontkanen, J., Dada, L., Kürten, A.,Yli-Juuti, T., Manninen, H., Amanatidis, S., Amorim, A., Baalbaki, R., Baccarini, A., Bell, D., Bertozzi, B., Bräkling, S., Brilke, S., Murillo, U. C., Chiu, R., Chu, B., De Menezes, L-P., Duplissy, J., Finkenzeller, H., Carracedo, L. G., Granzin, M., Guida, R., Hansel, A., Hofbauer, V., Krechmer, J., Lehtipalo, K., Lamkaddam, H., Lampimäki, M., Lee, C.P., Makhmutov, V., Marie, G., Mathot, S., Mauldin, R. L., Mentler, B., Müller, T., Onnela, A., Partoll, E., Petäjä, T., Philippov, M., Pospisilova, V., Ranjithkumar, A., Rissanen, M., Rörup, B., Scholz, W., Shen, J., Simon, M., Sipilä, M., Steiner, G., Stolzenburg, D., Tham, Y. J., Tomé, A., Wagner, A. C., Wang, D. S., Wang, Y., Weber, S.K., Winkler, P. M., Wlasits, P. J., Wu, Y., Xiao, M., Ye, Q., Zauner-Wieczorek, M., Zhou, X., Volkamer, R., Riipinen, I., Dommen, J., Curtius, J., Baltensperger, U., Kulmala, M., Worsnop, D. R., Kirkby, J., Seinfeld, J. H., El-Haddad, I., Flagan, R. C., and Donahue, N. M. (2020). Rapid growth of new atmospheric particles by nitric acid and ammonia condensation, Nature 581, 184–189, 2020b.

Wiedensohler, A., Cheng, Y.F., Nowak, A., Wehner, B., Achtert, P., Berghof, M., Birmili, W., Wu Z.J., Hu, M., Zhu, T., Takegawa, N., Kita, K., Kondo, Y., Lou, S.R., Hofzumahaus, A., Holland, F., Wahner, A., Gunthe, S.S, Rose, D., Su, H., Pöschl, U.(2009). Rapid aerosol particle growth and increase of cloud condensation nucleus activity by secondary aerosol formation and condensation: A case study for regional air pollution in northeastern china, J. Geophys. Res., 114, D00G08.

Wiedensohler, A., W. Birmili, A. Nowak, A. Sonntag, K. Weinhold, M. Merkel, B. Wehner, T. Tuch, S. Pfeifer, M. Fiebig, A. M. Fjaraa, E. Asmi, K. Sellegri, R. Depuy, H. Venzac, P. Villani, P. Laj, P. Aalto, J. A. Ogren, E. Swietlicki, P. Williams, P. Roldin, P. Quincey, C. Huglin, R. Fierz-Schmidhauser, M. Gysel, E. Weingartner, F. Riccobono, S. Santos, C. Gruning, K. Faloon, D. Beddows, R. M. Harrison, C. Monahan, S. G. Jennings, C. D. O'Dowd, A. Marinoni, H. G. Horn, L. Keck, J. Jiang, J. Scheckman, P. H. McMurry, Z. Deng, C. S. Zhao, M. Moerman, B. Henzing, G. de Leeuw, G. Loschau and S. Bastian (2012). "Mobility particle size spectrometers: harmonization

of technical standards and data structure to facilitate high quality long-term observations of atmospheric particle number size distributions." Atmospheric Measurement Techniques 5(3): 657-685.

Wiedensohler, A., A. Wiesner, K. Weinhold, W. Birmili, M. Hermann, M. Merkel, T. Muller, S. Pfeifer, A. Schmidt, T. Tuch, F. Velarde, P. Quincey, S. Seeger and A. Nowak (2018). "Mobility particle size spectrometers: Calibration procedures and measurement uncertainties." Aerosol Science and Technology 52(2): 146-164.

Zhang, R., Khalizov, A., Wang, L., Hu, M., and Xu, W. (2012). Nucleation and Growth of Nanoparticles in the Atmosphere, Chem. Rev., 112, 1957-2011, 2012.

Zhu, Y., Li, K., Shen, Y., Gao, Y., Liu, X., Yu, Y., Gao, H., and Yao, X. (2019). New particle formation in the marine atmosphere during seven cruise campaigns, Atmos. Chem. Phys., 19, 89–113.

Zhu, Y., Yan, C., Zhang, R., Wang, Z., Zheng, M., Gao, H., Gao, Y., and Yao, X. (2017) Simultaneous measurements of new particle formation at 1 s time resolution at a street site and a rooftop site, Atmos. Chem. Phys., 17, 9469–9484.

Anonymous Referee #4

This paper investigates long-term behavior of new particle formation (NPF) and associated particle growth at an elevated site. This is an important and scientifically very interesting topic, since there are quite limited number of studies about the response of NPF to SO2 emission reductions, and since the obtained results are somewhat mixed between different environments. The fact that the study is based on relatively short-term measurement campaigns made in different seasons, rather than continuous measurements over full years, limits the reliability of the obtained results, and this should be properly acknowledged in the paper. Anyway, I would support publication of this paper, provided that the authors will address the issues raised below.

Response: Thanks for the reviewer's comments. We agree that long-term continuous measurements would allow better investigating NPF trends under changing ambient conditions including air pollutants and meteorological factors. Due to practical difficulties, we tried short-term measurement campaigns made in different seasons of multiple years to characterize the NPF, with particular attention to the response of NPF to SO_2 emission. The limitations of the non-continuous measures and the uncertainties to explain the results have been added in the revised discussion. We also try our best to respond the comments and revise our manuscript accordingly.

Please note that after the major revisions of our manuscript, we have also made substantial changes in this response, and the language-editing have been processed in this version.

The introduction of this paper is generally well written. However, it would benefit from having a more concrete list of scientific questions aimed to addressed (in addition the aim mentioned on lines 75-76) in this paper. Two other, minor issues in this section: 1) the term "functions" on line 34 does not sound correct, perhaps "mechanisms"?, 2) the statement on line 74-75 is unclear. What altitudes are authors referring to here, above the boundary layer in general or upper free troposphere? One should be more careful with this, as elevated NPF can be associated with many different things, including convective uplift, presence of clouds, mixing of different air masses etc.

Response: Thanks. Lines 75-76 (lines 87-95 in this version) was revised as follow: "The main purpose of this study included: 1) to examine the effects of reduced SO_2 emissions on regional NPF events at a high altitude (from the upper boundary layer to the lower free troposphere), i.e., the changes in the NPF frequency, intensity and the subsequent growth of new particles; 2) to quantify the potential contribution of new particles to the CCN population and its changes under decreasing SO_2 emission; and 3) to rationalize the variation patterns of the NPF characteristics and CCN parameters in terms of observational concentrations of gaseous precursors and their origins and atmospheric behaviors. Note that all these changes in the study area should occur under the background of a rapid increase in BVOCs and their oxidized products as nucleating precursors

over the decades in China, although no studies can confirm the decadal increase in nucleating precursors from biogenic VOCs because of the lack of related analytic technologies in the past."

In the revision, we change ""functions" to "with different health and climate effects". On line 74 (line 86 in this version), we change "at higher elevations" to "above the boundary layer".

We agree that convective uplift, presence of clouds, mixing of different air masses, etc., may affect NPF events in clean remote atmospheres. We revise our discussion on the light of the issue.

Experimental methods have been described very shortly, and should be expanded a bit. How were the measurement data used in the current paper quality checked, are these data undergoing any quality assurance procedures? Did detection limits etc. cause any issues for data interpretations? Were there any serious gaps in the data during the periods chosen for the current study?

Response: Agree. The information will be added in the revised manuscript as following.

In revision, lines 118-127, we have added: "The WPS instrument was calibrated and/or repaired every 1-2 years by its vendor. The regular maintenance allowed the WPS to perform well, based on the recent comparison results of the WPS and a new scanning mobility particle sizer (SMPS, Grimm) in the summer of 2020, as shown in Fig. S3. The regular calibration parameters included the DMA sample/sheath flow, LPS sample/sheath flow, DMA/CPC pressure, DMA voltage, and DMA/ambient temperature. Polystyrene latex (PSL) spheres (NIST) with mean diameters of 100.7 nm and 269 nm were used for calibration. At the beginning of each campaign, the zero-points of the DMA, CPC, and LPS were checked using a purge filter at the inlet. Sometimes, the WPS operated improperly, and the data were excluded from the analysis (see the Fig. S4 for the occasional unexpected errors in three channels around 213 nm). In addition, we reproduced the $PM_{2.3}$ mass concentration from the WPS data and found that it was reasonably comparable to the measured $PM_{2.5}$, further supporting the accuracy of the WPS data. Details can be found in Fig. S5 and the supplementary materials."

In revision, lines 133-137, we have added: "For the analysers of SO_2, O_3, NO and NO_2, we performed multipoint calibrations every month and changed the filter every two weeks. The detection limits of SO_2, O_3, NO and NO_2 were 1 ppb, 0.4 ppb, 0.04 ppb, and 0.4 ppb, respectively. $PM_{2.5}$ was measured using a TEOM 1400a in 2007 and a Thermo 5030 SHARP after 2014. This device was calibrated by mass foil calibration according to the instrument manual, and the detection limit was 0.5 $\mu g/m^3$."

In revision, lines 140-143, we have added: "A multipoint calibration was performed for the online MARGA before and after the field campaigns to examine the sensitivity of the detectors. The detection limits were determined to be 0.05, 0.05, 0.04 and 0.05 $\mu g\ m^{-3}$ for Cl^-, NO_3^-, SO_4^{2-} and NH_4^+, respectively. More details about the instrument calibration can be found in Wen et al. (2018) and Li et al. (2020)."

Concerning the calculation methods, the authors should explicitly mention in main text (section

2.2.1) at which size particle formation rates were calculated, and what size range the calculated particle growth rates refer to (or if the applied size range for this calculation varied from event to event). Also, definition of "NPF duration" referred to e.g. on line 298 should explicitly described. Is it the time period over which new particles are observed to appear at the smallest sizes, or the time period over which the growth of new particle to larger sizes can be followed.

Response: Thanks. In revision, lines 166-168, we have added "The apparent FR of new particles is calculated based on nucleation mode particles with sizes of 10-25 nm. The GR is quantified by fitting the geometric median diameter of new particles (D_{pg}) during the whole particle growth period. The size range of D_{pg} varies from event to event."

The definition of "NPF duration" has been added in lines 157-164: "The initial time of an NPF event was defined as when new nucleation mode particles started to be observed (e.g., t_0 in Fig. 1b, d). The end time of an NPF event was defined as the new particle signal dropping to a negligible level and the total particle number concentrations approaching the background levels before the NPF event. In cases with the invasion of other plumes, the end time was determined to be when the new particle signals were suddenly overwhelmed by plumes and could no longer be identified (e.g., the end times in Fig. 1b, d). The NPF event duration was defined as the time duration between the initial time and end time of an NPF event. Note that the detection limit of WPS was 10 nm, but the particles were nucleated at critical cluster sizes of approximately 1-1.5 nm. Therefore, the NPF actually occurred at some time prior to our observation, and the actual duration should be longer than our calculation."

In addition, the schematic diagram of t_0 and end time, as well as other NPF parameters such as NMINP and ΔN_{CCN} has been added in Fig. 1 (as shown in Figure R1).

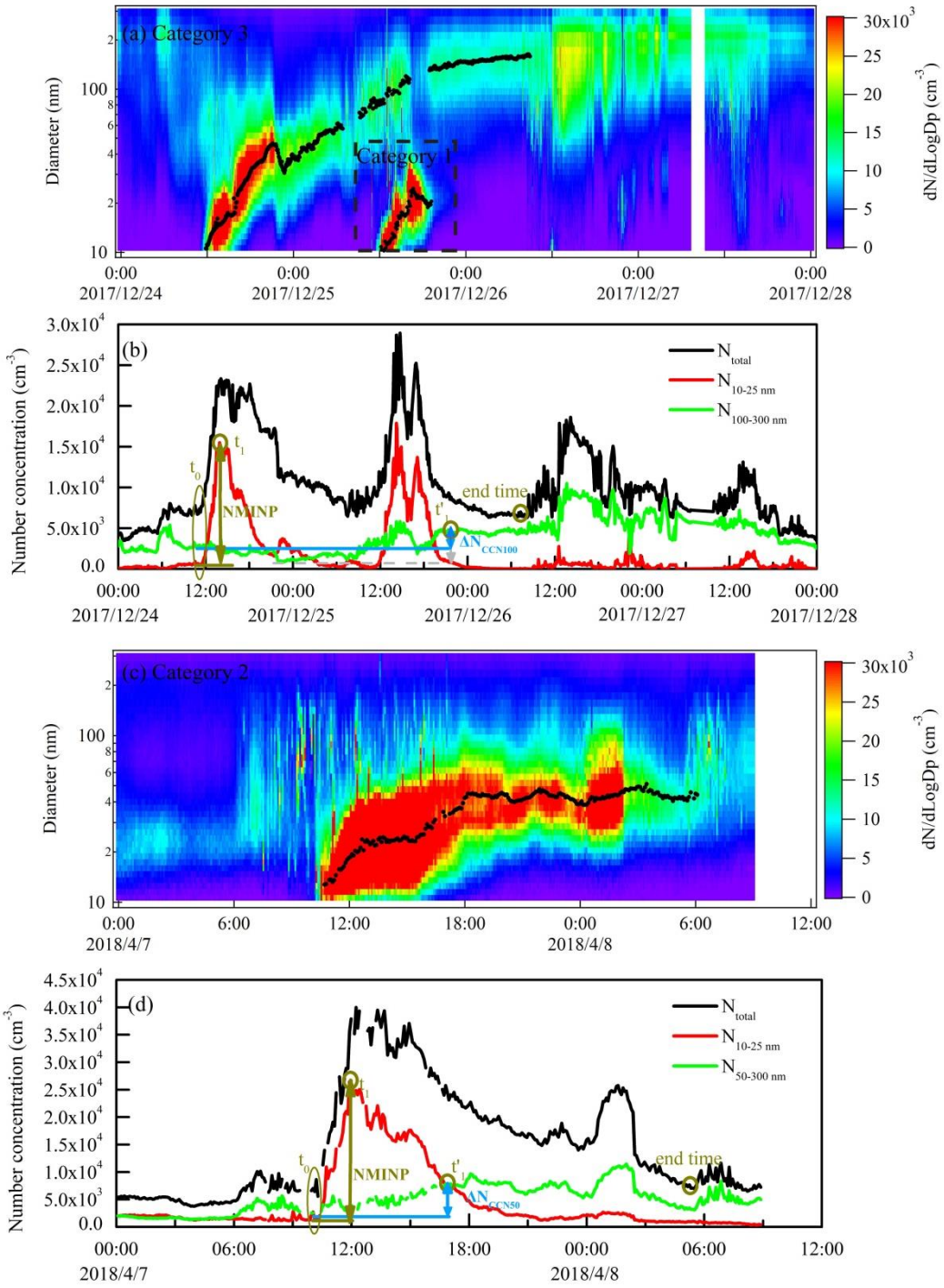

Figure R1 Examples of NPF events in three categories. Black dots in the figures are the fitted D_{pg}. (a) Category 1 on December 25, 2017, in which D_{pgmax} was 24 nm (<50 nm), and Category 3 on December 24, 2017, in which D_{pgmax} grew to 163 nm (>80 nm); (c) Category 2 on April 7, 2018, in which D_{pgmax} grew to 53 nm (50–80 nm). (b, d) Schematic diagram of t_0, t_1, t'_1, NMINP and $\Delta N_{CCN100}/\Delta N_{CCN50}$ on December 24, 2017 and April 7, 2018 NPF events (a few spikes have been removed from figure d).

Categorizing NPF event based on the maximum size that the formed particle are able to reach by

growth is in principle fine. However, doing that has one important issue that should be at least mentioned, and preferably shortly discussed, in the text. Following particle growth over several days, or event over the night, from observations is often difficult because of the typically large diurnal variation of boundary layer properties (e.g. mixed layer height), and because of changes in measured air masses. This can be seen, for example, on Dec 24 NPF event shown in Figure 1a: there are at least two major discontinuities in the particle number size distribution data (apparent in sudden huge changes in particle number concentration in certain size ranges). As a result, it is highly questionable whether the particles observed to reach 217 nm actually initiated from the NPF event that took place much earlier on Dec 24. The same issues concerns the use of the term SP (survival probability). SP works fine when following the particle growth for a few hours, but becomes questionable for larger time periods. The authors should replace the term "survival probability" with something like "apparent survival probability" and discuss shortly this issue in the paper, including when interpreting the results.

Response: In this study, D_{pgmax} and SP were calculated within the NPF duration. The definition of NPF duration has been clarified in the response above and has been added in the revision. In addition, a few spikes were excluded in calculating D_{pgmax} and SP since the spikes were characterized by a sudden change in particle number size distribution (PNSD) and may reflect primary particles from localized sources. These have been clarified in revision, lines 184-186.

As reported in numerous literatures, NPF was a regional phenomenon occurring in a spatial extent varies from tens to thousands of kilometers (Kulmala et al., 2012) However, it is almost impossible to occur identic NPF events over the large spatial range because of different concentration levels of nucleation precursors. In reverse, spatial heterogeneity of regional NPF events is a common phenomenon and would cause the discontinued PNSD to some extent at a fixed observational site.

No criteria have been well-established in the literature to identify spatial heterogeneity of NPF events. In this study, spatial heterogeneity of NPF events was assumed for the discontinued PNSD if no intrusion of primary or aged plume signals were clearly identified. Even though the intrusion of primary or aged plume signals overwhelmed new particle signals for a short period, new particle signals can still be reasonably observed afterwards in the contour plotting. The discontinued PNSD was also assumed as the continuity of the NPF event. The NPF event on Dec. 24 was illustrated as example:

On the Dec. 24 event, (Figure R1a-b), the two discontinuities in PNSD appeared at 7:00-9:00 and 16:10-18:50 on Dec. 25. From 22:48 on Dec. 24 to 7:00 on Dec. 25, N_{total} continuous decreased from 1.1×10^4 cm^{-3} to 0.8×10^4 cm^{-3}, meanwhile, D_{pg} grew from 30 nm to 63 nm with the growth rate of 4.0 nm/h. Between 7:00 and 9:00, $N_{10\text{-}300nm}$ and D_{pg} fluctuate at $0.8\pm0.1\times10^4$ cm^{-3} and 51±6 nm. At 9:00, $N_{10\text{-}300nm}$ and D_{pg} were 0.8×10^4 cm^{-3} and 72 nm, respectively. During the two hours (7:00-9:00), new particles were hypothesized to experience a growth similar to the previous curve. Similarly, D_{pg} was 115 nm at 16:10 and 128 nm at 18:50. The assumed growth rate during the 2.7 hours was about 4.8 nm/h, close to the previous GR. Actually, when we fitted the D_{pg} between 22:48 on Dec. 24 and 19:30 on Dec. 25, the GR was 4.8 nm/h and R^2=0.97, suggesting that particles grew in a smooth curve (Figure R2).

In this event, D_{pg} reached the maximum of 163 nm at 8:30 on Dec. 26, and then the new particle signals were overwhelmed by plumes after 9:00 on Dec. 26 (referred as end time). Followed equation (2), ΔN_{CCN} reached the maximum at 20:03 on 25 Dec. The SP was calculated as $SP = \Delta N_{CCN}/NMINP$, and SP_{CCN50}, SP_{CCN80}, and SP_{CCN100} was calculated to be 0.2, 0.2 and 0.15, respectively. However, Figure R1b also shows that the choice of t_0 may lead to underestimation of ΔN_{CCN} to some extent in the presence of spatial-temporal heterogeneity of pre-existing particles with diameters larger than 50 nm. In these cases, the mean value of N_{CCN} in the percentiles smaller than 5th during the whole NPF event may be more accurate representing the background (see the grey dashed line in Figure R1b). However, this method may also introduce more subjective factors and therefore was not adopted in this study. These have been clarified in the revision (lines 214-218).

We agree to change "survival probability" to "apparent survival probability". The judgment of spatial heterogeneity in other NPF events followed the similar approach above, and we have add the discussion of spatial heterogeneity in the revised manuscript, lines 209-211: "Note that the spatial-temporal heterogeneity during NPF events may result in high SPs. If the observed ΔN_{CCN} exceeded NMINP and the calculated SPs exceeded 100%, suggesting equation (3) was not applicable in these cases, and SP was therefore not calculated."

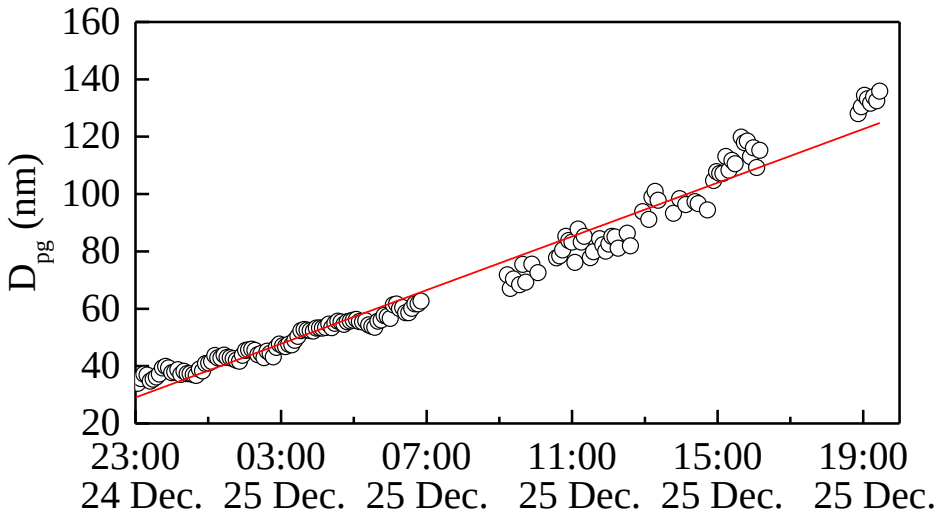

Figure R2 Growth curve of the fitting the geometric median diameter of new particles (D_{pg}) from 22:48 on Dec. 24 to 19:30 on Dec. 25.

The authors should be a bit more careful when using the term "trend". On line 191, for example, should there read "pattern" rather than "trend"? Multi-year trends can be season-dependent, but I suppose this not what the authors mean here. Please check out that "trend" is correctly used throughout the paper.

Response: Thanks. We agree the reviewer's comment that "trend" was inappropriate in this paragraph. Our main purpose was to examine the effects of reduced SO_2 emissions on the regional NPF events characteristics and the CCN parameters. We have change "trend" to "pattern" in this sentence and go through the full text and revise the ambiguous statements.

Reference:

Kulmala, M., Petäjä, T., Nieminen, T., Sipilä, M., Manninen, H. E., Lehtipalo, K., Dao Maso, M., Aalto, P. P., Junninen, H., Paasonen, P., Riipinen, I., Lehtinen, K. E. J., Laaksonen, A., and Kerminen, V-M.: Measurement of the nucleation of atmospheric aerosol particles, Nat. Protoc., 7, 1651–1667, https://doi.org/10.1038/nprot.2012.091, 2012.

Li, H. Y., Zhu, Y. J., Zhao, Y., Chen, T. S., Jiang, Y., Shan, Y., Liu, Y. H., Mu, J. S., Yin, X. K., Wu, D., Zhang, C., Si, S. C., Wang, X. F., Wang, W. X., Xue, L. K. Evaluation of the Performance of Low-Cost Air Quality Sensors at a High Mountain Station with Complex Meteorological Conditions, Atmosphere, 11, 212; doi:10.3390/atmos11020212, 2020.

Wen, L., Xue, L., Wang, X., Xu, C., Chen, T., Yang, L., Wang, T., Zhang, Q., and Wang, W.: Summertime fine particulate nitrate pollution in the North China Plain: increasing trends, formation mechanisms and implications for control policy, Atmos. Chem. Phys., 18, 11261–11275, https://doi.org/10.5194/acp-18-11261-2018, 2018.

Increased new particle yields with largely decreased probability of survival to CCN size at the summit of Mt. Tai under reduced SO_2 emissions

Yujiao Zhu[1], Likun Xue[1,2*], Jian Gao[3], Jianmin Chen[4], Hongyong Li[1], Yong Zhao[5], Zhaoxin Guo[5], Tianshu Chen[1], Liang Wen[1], Penggang Zheng[1], Ye Shan[1], Xinfeng Wang[1], Tao Wang[6], Xiaohong Yao[7*], Wenxing Wang[1]

[1]Environment Research Institute, Shandong University, Qingdao 266237, China

[2]Collaborative innovation Center for climate Change, Jiangsu Province, Nanjing, 210023, China

[3]Chinese Research Academy of Environmental Sciences, Beijing 100012, China

[4]Shanghai Key Laboratory of Atmospheric Particle Pollution and Prevention (LAP3), Department of Environmental Science & Engineering, Fudan University, Shanghai 200433, China

[5]Taishan National Reference Climatological Station, Tai'an 271000, China

[6]Department of Civil and Environmental Engineering, Hong Kong Polytechnic University, Hong Kong, China

[7]Key Lab of Marine Environmental Science and Ecology, Ministry of Education, Ocean University of China, Qingdao 266100, China

Correspondence to: Likun Xue (xuelikun@sdu.edu.cn) and Xiaohong Yao (xhyao@ouc.edu.cn)

Abstract. Because anthropogenic sulfur dioxide (SO_2) emissions have decreased considerably in the last decade, $PM_{2.5}$ pollution in China has been alleviated to some extent. However, the effects of reduced SO_2 on the particle number concentrations and subsequent contributions of grown new particles to cloud condensation nuclei (CCN) populations, particularly at high altitudes with low aerosol number loadings, are poorly understood. In contrast, the large increase in provincial forest areas with the rapid afforestation in China over the last decades expectedly increases the biogenic emissions of volatile organic compounds and their oxidized products as nucleating precursors therein. In this study, we evaluated the campaign-based measurements made at the summit of Mt. Tai (1534 m a.s.l.) from 2007 to 2018. With the decrease in the SO_2 mixing ratios from 15 ± 13 ppb in 2007 to 1.6 ± 1.6 ppb in 2018, the apparent formation rate of new particles (FR) and the net maximum increase in the nucleation-mode particle number concentration (NMINP) in the spring campaign of 2018 was 2–3 fold higher than those in the spring campaign of 2007, with almost the same occurrence frequency of new particle formation (NPF) events. In contrast, the campaign-based comparison showed that the occurrence frequency, in which the maximum geometric median diameter of the grown new particles (D_{pgmax}) was >50 nm, decreased considerably, from 43%–78% of the NPF events before 2015 to <12% in 2017–2018. Assuming >50 nm as a CCN threshold size at high supersaturations, the observed net CCN production decreased from 3.7×10^3 cm^{-3} (on average) in the five campaigns before 2015 to 1.0×10^3 cm^{-3} (on average) in the two campaigns in 2017–2018. We argue that the increases in the apparent FR and NMINP are mainly determined by the availability of organic precursors that participate in nucleation and initial growth,

whereas the decrease in the growth probability is caused by the reduced emissions of anthropogenic precursors. However, large uncertainties still exist because of a lack of data on the chemical composition of these smaller particles.

1. Introduction

Atmospheric new particle formation (NPF) is regarded as an important source of aerosol particles in terms of number concentrations, and the newly formed particles can grow into a variety of sizes, with different health and climate effects. For example, particles larger than 50–80 nm may act as cloud condensation nuclei (CCN), whereas those larger than 100 nm may directly affect solar radiation (Kulmala and Kerminen, 2008; Kerminen et al., 2012; Seinfeld and Pandis, 2012). Sulfuric acid (H_2SO_4) is considered as the key nucleating precursor for NPF, and other species, such as ammonia (NH_3), amines, and highly oxygenated molecules [HOMs—oxidation products of volatile organic compounds (VOCs)], can also participate and enhance nucleation in the continental troposphere (Ehn et al., 2014; Tröstl et al., 2016; Yao et al., 2018; Kerminen et al, 2018; Chu et al., 2019; Lee et al., 2019). The subsequent growth of new particles is affected by not only the abovementioned precursors but also the semivolatile compounds (Riipinen et al., 2012; Ehn et al., 2014; Tröstl et al., 2016).

NPF events have been reported widely throughout the world, including in severely polluted urban and rural areas in China that experience high sulfur dioxide (SO_2) concentrations and high aerosol loading (Kulmala et al., 2004; Gao et al., 2009; Guo et al., 2012; Nie et al., 2014; Kerminen et al., 2018; Chu et al., 2019). In the last few decades, anthropogenic emissions of gaseous and particulate air pollutants in China have been reduced substantially due to rigorous emission control policies. Between 2007 and 2018 (the observation period in this study), the national total SO_2 emissions decreased by 67% (from 24.7 million tons to 8.2 million tons), and the national average ambient SO_2 concentrations decreased by 73% (from 17.9 ppb to 4.9 ppb; see Fig. S1). The North China Plain (NCP) region experiences the most severe SO_2 pollution, which has visibly decreased trend since 2011 (Krotkov et al., 2016; Fan et al., 2020). Such huge reductions in SO_2 emissions may alter the frequency and intensity of NPF events and the subsequent growth of new particles. The changes in the mixing ratios of VOC components, ambient oxidants, aerosol loading, and meteorological factors may also influence NPF events, yielding more complex and uncertain feedback (Kulmala and Kerminen, 2008; Zhang et al., 2012).

The long-term changes in NPF events under lower SO_2 conditions have been studied in several cities in Europe and the U.S. For example, decreased NPF frequency and reduced new particle yields were associated with decreases in SO_2 concentrations in Pittsburgh (U.S.), Rochester (U.S.), and Melpitz (Germany) (Hamed et al., 2010; Wang et al., 2011, 2017; Saha et al., 2018). In contrast, long-term studies in Pallas (Finland), Hyytiälä (Finland), and Crete (Greece) observed no trends in NPF frequencies despite considerable decreases in the ambient SO_2 concentrations all over Europe (Asmi et al., 2011; Nieminen et al., 2014; Kalivitis, et al., 2019). Moreover, a slight upward trend in the particle formation and growth rates was observed in Pallas and Hyytiälä, attributable to the increased biogenic VOC (BVOC) emissions (Asmi et al., 2011; Nieminen et al., 2014).

In China, the earliest observation of NPF events started in approximately around 2004 in Beijing (Wu et al., 2007). Comparison of tens of independent experiments showed that the NPF frequency has remained relatively constant until recent years, possibly due to the reduced production and reduced loss rate of H_2SO_4; these phenomena may have canceled each other out to some extent in Beijing (Chu et al., 2019; Li et al., 2020). In addition, a recent study reported that China has experienced rapid afforestation, with provincial forest areas increasing by between 0.04 million and 0.44 million hectares per year over the past 10 to 15 years, leading to a large increase in the CO_2 sink based on long-term observations over large spatial scales (Wang et a., 2020). BVOC emissions in China are reasonably expected to greatly increase over the past 15 years. Considering the key roles of oxidized BVOCs in NPF events (Riipinen et al., 2012; Ehn et al., 2014; Tröstl et al., 2016; Chu et a., 2019), the responses of NPF in China, in terms of their occurrence frequency, intensity and potential impacts on the climate, to reduced anthropogenic SO_2 emissions may not be the same as those observed in Europe and North America. However, the long-term changes in NPF intensities and the subsequent growth of new particles have not been studied in China, where the anthropogenic emissions of various air pollutants and biogenic emissions of VOCs have been changing significantly in opposite directions in the past decade.

In this study, we analyzed the measurement data of particle number concentrations, chemical compositions, trace gases, and meteorological parameters collected at the summit of Mt. Tai (36.25°N, 117.1°E, 1534 m a.s.l.) during seven observational campaigns from 2007 to 2018. Mt. Tai is the highest mountain in the NCP, located at the region's center, and the observation station has been widely deployed to investigate regional air pollution as well as transport and chemical processes in the NCP (Gao et al., 2005; Li et al., 2011; Sun et al., 2016; Wen et al., 2018). Moreover, the summit is close to the top of the planetary boundary layer or even in the free troposphere sometimes, and is characterized by relatively few pre-existing particles, strong UV solar radiation, and low ambient temperature, which favor NPF events (Li et al., 2011; Shen et al., 2016a; Lv et al., 2018;). The tree coverage areas around the sampling site evidently increased from 2003 to 2016 based on MODIS satellite data (Fig. S2). The contribution of new particles, compared with that of primary particles, to the CCN population reportedly increases above the boundary layer, indicating a critical role of high-altitude NPF in cloud formation and the related climate impacts (Merikanto et al., 2009). The main purpose of this study included: 1) to examine the effects of reduced SO_2 emissions on regional NPF events at a high altitude (from the upper boundary layer to the lower free troposphere), i.e., the changes in the NPF frequency, intensity and the subsequent growth of new particles; 2) to quantify the potential contribution of new particles to the CCN population and its changes under decreasing SO_2 emission; and 3) to rationalize the variation patterns of the NPF characteristics and CCN parameters in terms of observational concentrations of gaseous precursors and their origins and atmospheric behaviors. Note that all these changes in the study area should occur under the background of a rapid increase in BVOCs and their oxidized products as nucleating precursors over the decades in China, although no studies can confirm the decadal increase in nucleating precursors from biogenic VOCs because of the lack of related analytic technologies in the past.

2. Methods

2.1 Experimental

This study comprised seven intensive campaigns from 2007 to 2018, and the details are summarized in Table 1. The duration of each campaign varied from 18 days to 71 days. The measurement data obtained in the four campaigns in 2007, 2014, and 2015 have been reported by Gao et al. (2008) and Lv et al. (2018), and here, all of the available data were combined to examine the effects of reduced SO_2 emissions on regional NPF events.

All measurements were obtained using commercial instruments, which were housed in a container and have been described in previous studies (e.g., Zhou et al., 2009; Zhu et al., 2017; Lv et al., 2018). During the seven campaigns, the particle number size distributions (PNSDs) were monitored using a wide-range particle spectrometer (*WPS; Model 1000XP, MSP Corporation, USA*) at ambient relative humidity (RH). Conductive tubes (TSI 1/4 in.) were used for the WPS sampling, and the length of the tube was kept at approximately 2 m in each campaign. The WPS combines a differential mobility analyzer (DMA), a condensation particle counter (CPC), and a laser particle spectrometer (LPS). The DMA and CPC can measure particles in the 10–500 nm (or 5–500 nm in the advance mode) size range and were set up to 48 channels. The SWS mode (DMA operating in the voltage-scanning mode) was selected. The LPS covers the size range of 350 nm–10 μm and is divided into 24 channels. In this study, the detection limit of the DMA was 10 nm in 2007 and 2009, while it was 5 nm in 2014, 2015, 2017, and 2018. For consistency, the particles sized 10–300 nm were used for the calculations in all campaigns except for that in spring of 2007, when the data of >153 nm particles were missing, so we used the data of 10–153 nm particles instead for calculation. The net increases in the number concentrations of 10-25 nm particles during the initial several hours of NPF events were over 1~2 orders of magnitude in this study, e.g., in Fig. 1b, d. The uncertainties of the measured particle number concentrations at approximately 10 nm in 2007 and 2009 and those after had a negligible influence on the net increases. In addition, the use of the 10-153 nm particles in 2007 may lead to underestimation of the particle number concentration, as detailed in the supplementary materials

The WPS instrument was calibrated and/or repaired every 1-2 years by its vendor. The regular maintenance allowed the WPS to perform well, based on the recent comparison results of the WPS and a new scanning mobility particle sizer (SMPS, Grimm) in the summer of 2020, as shown in Fig. S3. The regular calibration parameters included the DMA sample/sheath flow, LPS sample/sheath flow, DMA/CPC pressure, DMA voltage, and DMA/ambient temperature. Polystyrene latex (PSL) spheres (NIST) with mean diameters of 100.7 nm and 269 nm were used for calibration. At the beginning of each campaign, the zero-points of the DMA, CPC, and LPS were checked using a purge filter at the inlet. Sometimes, the WPS operated improperly, and the data were excluded from the analysis (see the Fig. S4 for the occasional unexpected errors in three channels around 213 nm). In addition, we reproduced the $PM_{2.3}$ mass concentration from the WPS data and found that it was reasonably comparable to the measured $PM_{2.5}$, further supporting the accuracy of the WPS data. Details can be found in Fig. S5 and the supplementary materials.

The trace gases were monitored during each campaign. SO_2 was measured using an ultraviolet fluorescence analyzer (*Model 43C, Thermo Electron Corporation, USA*); O_3 was monitored using two ultraviolet absorption analyzers (*Model 49C, Thermo Electron Corporation, USA*, or *Model 400U, Advanced Pollution Instrumentation Inc., USA*); NO and NO_2 were monitored using a chemiluminescence analyzer (*Model 42C or 42i, Thermo Electron Corporation, USA*) equipped with a blue light converter before August 2014 and subsequently using a chemiluminescence analyzer (*Model T200U, API, USA*) and a cavity-attenuated phase-shift spectroscopy instrument (*Model T500U, API, USA*), respectively. For the analysers of SO_2, O_3, NO and NO_2, we performed multipoint calibrations every month and changed the filter every two weeks. The detection limits of SO_2, O_3, NO and NO_2 were 1 ppb, 0.4 ppb, 0.04 ppb, and 0.4 ppb, respectively. $PM_{2.5}$ was measured using a TEOM 1400a in 2007 and a Thermo 5030 SHARP after 2014. This device was calibrated by mass foil calibration according to the instrument manual, and the detection limit was 0.5 $\mu g/m^3$. The inorganic water-soluble ions in $PM_{2.5}$ together with the acid and alkaline gases were measured using an online Ambient Ion Monitor (*URG-AIM 9000B, URG Corporation, USA*; only for water-soluble ions in $PM_{2.5}$) in 2007 and using a Monitor for Aerosols and Gases (*MARGA; ADI20801, Applikon-ECN, Netherlands*) in the five campaigns from 2014 onward. A multipoint calibration was performed for the online MARGA before and after the field campaigns to examine the sensitivity of the detectors. The detection limits were determined to be 0.05, 0.05, 0.04 and 0.05 $\mu g\ m^{-3}$ for Cl^-, NO_3^-, SO_4^{2-} and NH_4^+, respectively. More details about the instrument calibration can be found in Wen et al. (2018) and Li et al. (2020). Data on the meteorological parameters including temperature (T), RH, wind speed, wind direction, and precipitation were provided by the Mt. Tai Meteorological Station.

The air mass back trajectories were calculated using the Hybrid Single Particle Lagrangian Integrated Trajectory (HYSPLIT) model. The input meteorological data [Global Data Analysis System (GDAS) data] were used with a 1° latitude–longitude resolution. A trajectory ending height of 1400 m a.g.l. was selected because the terrain height on Mt. Tai was approximately 150 m in the GDAS data.

2.2 Calculation methods

2.2.1 Definition of NPF events and relevant parameters

In this study, particles with diameters smaller than 25 nm were defined as nucleation mode particles (Kulmala et al., 2012). Following the criteria proposed by Dal Maso et al. (2005) and Kulmala et al. (2012), three features had to be met for an event to qualify as NPF: 1) a distinctly new nucleation mode particles must appear in the size distribution; 2) the new mode should prevail over a time span of hours; and 3) the new mode should show signs of growth. All three features are required for a day (00:00-23:59 LT) to be classified as an NPF day. Otherwise, the day is classified as a non-NPF day.

The initial time of an NPF event was defined as when new nucleation mode particles started to be observed (e.g., t_0 in Fig. 1b, d). The end time of an NPF event was defined as the new particle signal dropping to a negligible level and the total particle number concentrations approaching the background levels before the NPF event. In cases with the invasion of other

plumes, the end time was determined to be when the new particle signals were suddenly overwhelmed by plumes and could no longer be identified (e.g., the end times in Fig. 1b, d). The NPF event duration was defined as the time duration between the initial time and end time of an NPF event. Note that the detection limit of WPS was 10 nm, but the particles were nucleated at critical cluster sizes of approximately 1-1.5 nm. Therefore, the NPF actually occurred at some time prior to our observation, and the actual duration should be longer than our calculation.

Three parameters are commonly used to evaluate NPF characteristics, viz., apparent formation rate (FR), growth rate (GR), and condensation sink (CS) (Sihto et al., 2006; Kulmala et al., 2012). The apparent FR of new particles is calculated based on nucleation mode particles with sizes of 10-25 nm. The GR is quantified by fitting the geometric median diameter of new particles (D_{pg}) during the whole particle growth period. The size range of D_{pg} varies from event to event. Details of the calculation equations can be found in the supplementary materials. Note that the lack of measurements of >153 nm particles in the spring campaign of 2007 may lead to an underestimation of the CS. We tested the possible underestimation using the data measured in 2018 by comparing the CS values calculated for the measured number concentrations of particles in the 10-153 nm, 10-300 nm and 10-2500 nm size ranges. The use of the 10-153 nm particles may lead to ~50% underestimation of the CS compared to that using the 10-2500 nm particles. Thus, the CS value from the 10-153 nm particles in the spring campaign of 2018 was compared with that obtained in the spring campaign of 2007. However, the CS values from the 10-300 nm particles accounted for 94% of those from the 10-2500 nm particles. Thus, the CS values from the 10-300 nm particles were used throughout the study, except in 2007.

Another two metrics were applied to characterize the NPF events, i.e., the net maximum increase in the nucleation-mode particle number concentration (NMINP), and the maximum size of D_{pg} (D_{pgmax}). The two metrics were proposed in our previous studies (Zhu et al., 2017, 2019). The NMINP indicated the intensity of an NPF event, which was calculated as:

$$\mathrm{NMINP} = N_{10\text{–}25\ \mathrm{nm}}(t_1) - N_{10\text{–}25\ \mathrm{nm}}(t_0) \quad (1)$$

where $N_{10\text{–}25\ \mathrm{nm}}$ is the sum of the nucleation mode particle number concentrations, and t_0 and t_1 represent the time when an NPF event is initially observed and the time when $N_{10\text{–}25\ \mathrm{nm}}$ reaches the maximum value, respectively. Fig. 1b, d shows the schematic diagram of the NMINP.

Note that a few spikes were occasionally observed with a broader particle number size distribution during the NPF period. These spikes were excluded in the calculation of the FR, GR, D_{pg}, NMINP and CCN parameters (described in 2.2.2) because they may reflect primary particles from localized sources (Liu et al., 2014; Man et al., 2015; Zhu et al., 2017).

According to the different sizes of D_{pgmax}, the NPF events were classified into three categories (as shown in Fig. 1). In Category 1 events (e.g., December 25, 2017, Fig. 1a), the new particles grow to a D_{pgmax} of <50 nm and are too small to serve as CCN. In Category 2 events (e.g., April 7, 2018, Fig. 1b), the new particles grow to a D_{pgmax} of 50–80 nm. In Category 3

events (e.g., December 24, 2017, Fig. 1a), the new particles grow to D_{pgmax} of >80 nm. The NPF events in Categories 2 and 3 can be regarded as climate-relevant events.

2.2.2 CCN parameters

In the absence of direct CCN measurements, the potential contribution of new particles to the CCN population can be estimated from the particle number size distribution (Lihavainen et al., 2003; Rose et al., 2017). Theoretically, particles larger than 50 nm (i.e., 80 nm) can be activated as CCN under quite high (moderate) supersaturation (Dusek et al., 2006; Petters and Kreidenweis, 2007; Ma et al., 2016), and particles larger than 100 nm can directly impact the climate by scattering and absorbing solar radiation (Charlson et al., 1992; Seinfeld and Pandis, 2012). In this study, we introduced three terms: the net increase in the NPF-derived CCN number concentration (ΔN_{CCN}), the apparent survival probability of new particles to the CCN sizes (SP), and the relative increase ratio of the CCN population (R_{CCN}). Three sizes, viz., 50 nm, 80 nm, and 100 nm, were defined as the CCN threshold sizes. ΔN_{CCN} was calculated following the method of Rose et al. (2017):

$$\Delta N_{CCN} = N_{CCN}(t'_1) - N_{CCN}(t_0) \quad (2)$$

where the N_{CCN} terms represent the potential CCN number concentrations and were estimated from the number concentrations of particles larger than 50 nm, 80 nm, and 100 nm (N_{CCN50}, N_{CCN80}, and N_{CCN100}, respectively); t_0 is the time when an NPF event is initially observed, the same as that in equation (1); and t'_1 is the time when N_{CCN} reaches the maximum value during the new particle growth periods. Each concentration was taken as a 1-h average. The ΔN_{CCN} term eliminates the influence of pre-existing particles. A schematic diagram of N_{CCN100} and N_{CCN50} can be found in Fig. 1b, d.

The SP was calculated as described by Zhu et al. (2019):

$$SP = \Delta N_{CCN}/NMINP \quad (3)$$

Note that the spatial-temporal heterogeneity during NPF events may result in high SPs. If the observed ΔN_{CCN} exceeded NMINP and the calculated SPs exceeded 100%, suggesting equation (3) was not applicable in these cases, and SP was therefore not calculated.

The R_{CCN} values were the ratios of the NPF-derived CCN to the pre-existing CCN and were calculated as follows:

$$R_{CCN} = \Delta N_{CCN}/N_{CCN}(t_0) \quad (4)$$

Moreover, Fig. 1b shows that the choice of t_0 may lead to underestimation of ΔN_{CCN} to some extent in the presence of spatial-temporal heterogeneity of pre-existing particles with diameters larger than 50 nm. In these cases, the mean value of N_{CCN} in the percentiles smaller than 5th during the whole NPF event may be more accurate representing the background (see the grey dashed line in Fig. 1 b). However, this method may also introduce more subjective factors and therefore was not adopted in this study.

In addition, the maximum geometric median diameter of the grown new particles never exceeded 89 nm in spring 2007. Considering the log-normal distribution of the grown new particles, the number concentration of grown new particles with diameters >153 nm was less than 15% (Fig. S6). Thus, it is safe to say that the lack of data for >153 nm particles had a negligible effect on the calculated ΔN_{CCN50}, ΔN_{CCN80} and ΔN_{CCN100} in 2007.

2.2.3 Sulfuric acid proxy

The proxy for the H_2SO_4 concentration could be roughly estimated based on the solar radiation (SR), SO_2 concentration, CS, and RH as follows (Mikkonen et al., 2011; Lv et al., 2018):

$$[H_2SO_4] = 8.21 \times 10^{-3} \cdot k \cdot SR \cdot [SO_2]^{0.62} \cdot (CS \cdot RH)^{-0.13} \quad (5)$$

where k is a temperature-dependent reaction rate constant, and SR was estimated from the HYSPLIT model.

The contribution of H_2SO_4 vapor to the particle growth from D_{p0} to D_{p1} can be expressed by the following equation (Kulmala et al., 2001):

$$R = ([H_2SO_4]_{avg}/C) \times 100\% \quad (6)$$

where $[H_2SO_4]_{avg}$ is the average concentration of H_2SO_4 during the particle growth period, and C is the total concentration of condensable vapor for the particle growth from D_{p0} to D_{p1}, which can be calculated as described by Kulmala et al. (2001). Notably, uncertainty may exist in the estimated contribution of the SO_2 concentrations and radiation intensity to H_2SO_4, as well as in the contribution of H_2SO_4 to the particle growth.

3. Results

3.1 Variation in the NPF frequency

During the seven campaigns, NPF events were observed on 106 of the 265 sampling days. As shown in Fig. 2, the NPF frequencies in the three seasons of different years were surprisingly almost the same, i.e., 50% in the spring of 2007, 50% in the summer of 2009, 49% in the winter of 2017, and 51% in the spring of 2018. However, the NPF frequency decreased to 42% in the summer of 2014, 33% in the fall of 2014, and 20% in the summer of 2015. The low NPF frequencies were likely caused by perturbations from meteorological conditions. For example, there were 15 rainy days out of the 40 sampling days during the 2015 summer campaign, but only 3 rainy days out of the total 18 sampling days in the 2009 summer campaign. Moreover, the solar radiation averaged over the 2009 summer campaign was 1.4 times that of the 2015 summer campaign

(Fig. S7). These factors may have caused the NPF frequency in the 2009 summer campaign to be close to that in the other season campaigns but that of the 2015 summer campaign to be lower.

When Categories 1, 2, and 3 of the NPF events were examined separately, the Category 1 NPF frequencies in the winter of 2017 (43%) and the spring of 2018 (49%) were significantly higher than those before (5%–21%; $p < 0.05$). Category 2 events were absent in the winter of 2017, whereas Category 3 events were absent in the spring of 2018. The sums of the Category 2 and 3 NPF frequencies in 2017 (6%) and 2018 (3%) were significantly lower than those before (14%–39%; $p < 0.05$), even in comparison with the relatively low NPF frequencies in the summer of 2015 (15%) and the fall of 2014 (14%). When the sums of the Category 2 and 3 NPF frequencies in each campaign were normalized by the corresponding total NPF frequency, the boundary was clearer, i.e., the normalized sum values were as high as 43%–78% before 2015 and <12% in 2017–2018. Clearly, the newly formed particles observed at Mt. Tai in 2017–2018 were less climatically relevant than those before 2015 (64-78% in the three summer campaigns versus 43% and 59% in the fall and spring campaigns), despite the comparable NPF frequencies.

3.2 Variations in the apparent FR, NMINP, GR, and D_{pgmax}

We used four metrics, i.e., the apparent FR, NMINP, GR, and D_{pgmax}, to characterize the NPF events and evaluate the potential climate impacts of the grown new particles (Fig. 3). During the four campaigns in 2007, 2009, and 2014, the calculated apparent FR varied narrowly in each campaign and the campaign average narrowed to 0.8–1.2 cm^{-3} s^{-1}. The apparent FR increased in the three subsequent campaigns, i.e., 2.6 ± 1.3 cm^{-3} s^{-1} in 2015, 2.0 ± 1.7 cm^{-3} s^{-1} in 2017, and 3.0 ± 2.7 cm^{-3} s^{-1} in 2018. The apparent FRs were 3–7 times lower than those obtained from the measurements with a lower limit of 3 nm of the twin differential mobility particle sizer (TDMPS) and neutral cluster and air ion spectrometer (NAIS) at the same site during previous campaigns (Shen et al., 2016a,b; Lv et al., 2018).

The NMINP showed a temporal variation pattern similar to that of the apparent FR (Fig. 3b). The campaign average NMINP varied in a narrow range of 3.8–5.1 × 10^3 cm^{-3} in 2007–2014, but then increased to 6.3 ± 2.6 × 10^3 cm^{-3} in 2015, 9.4 ± 7.9 × 10^3 cm^{-3} in 2017, and 1.1 ± 1.0 × 10^4 cm^{-3} in 2018. The increase in the NMINP should enhance the contribution of NPF events to the ambient particle number concentration, but the NMINP at Mt. Tai before 2015 was only approximately ¼–½ of those of our previous observations in urban and marine atmospheres (Zhu et al., 2017, 2019).

The variations in GR were strongly seasonally dependent (Fig. 3c). Higher GRs were generally observed in the summer campaigns, with the three campaign averages in the range of 7.3–9.6 nm h^{-1}. The higher GRs in summer were due to the higher photochemical reactions and biological activities, which is consistent with those reported in the literature (Kulmala et al., 2004; Chu et al., 2019). The reverse was true in winter, and a lower GR was expectedly observed in the winter of 2017, i.e., 2.3 ± 1.3 nm h^{-1}. The GRs in the fall and spring campaigns ranked between those of the summer and winter campaigns. For example, the average GR was 4.9 ± 2.7 nm h^{-1} in the fall of 2014. The average GR in the spring of 2007 (4.4 ± 2.3 nm

h^{-1}) was slightly higher than that in the spring of 2018 (3.3 ± 2.3 nm h^{-1}), although the apparent FR and NMINP increased considerably in the latter spring campaign.

The D_{pgmax} is partially determined by the GR. The largest campaign average D_{pgmax} of 84 ± 39 nm appeared as expected in the summer of 2009, followed by 71 ± 24 nm in the summer of 2015. However, the campaign average D_{pgmax} was only 60 ± 18 nm in the summer of 2014, followed by 57 ± 16 nm in the spring of 2007, 53 ± 22 nm in the fall of 2014, and 40 ± 40 nm in the winter of 2017. The campaign average D_{pgmax} in the spring of 2018 was the lowest, i.e., 29 ± 13 nm, although the campaign average GR was even larger than that in the winter of 2017. These findings indicate that D_{pgmax} is clearly determined not only by the GR but also by unidentified factors, which is addressed in Section 4.2.

In summary, we found that the apparent FR and NMINP in the spring campaign of 2018 were higher than those of 2007. The GR showed strong seasonal dependence. The D_{pgmax} was significantly lower in 2018, but the GR alone could not explain the lower values.

3.3 Potential contribution to CCN production from the NPF events

Direct measurements of the CCN were not available; therefore, the potential contributions of the grown new particles to the CCN population were estimated using equations (2)–(4). The contributions varied considerably between campaigns (Fig. 4). In general, the NPF-derived CCNs were seasonally dependent, i.e., the highest number concentrations occurred in summer, followed by spring, fall, and winter. With an increase in the threshold diameters, roughly corresponding to a decrease in supersaturation from >0.6% to <0.1% (Li et al., 2015), the estimated contributions decreased because new particles were continuously removed either by coagulation or atmospheric deposition during the particle growth. During the three summer campaigns in 2009, 2014, and 2015, larger NPF-derived CCNs were estimated with average ΔN_{CCN50}, ΔN_{CCN80}, and ΔN_{CCN100} values of 4.4 ± 2.5 × 10^3 cm^{-3}, 1.9 ± 1.5 × 10^3 cm^{-3}, and 1.0 ± 0.9 × 10^3 cm^{-3}, respectively. Overall, the values decreased by approximately 50% in the spring of 2007 and the fall of 2014. The NPF-derived CCNs in these five campaigns were larger than those reported in previous studies for the same season at Mt. Chacaltaya (5240 m, Bolivia) and Botsalano (1424 m, South-Africa) (Kerminen et al., 2012; Rose et al., 2017). In comparison, extremely low NPF-derived CCNs were observed in 2017 and 2018, i.e., ΔN_{CCN50} of only 1.1 ± 1.7 × 10^3 cm^{-3}, ΔN_{CCN80} of 0.5 ± 0.9 × 10^3 cm^{-3}, and ΔN_{CCN100} of 0.2 ± 0.5 × 10^3 cm^{-3}.

High SPs were found during the three summer campaigns in 2009, 2014, and 2015, with average SP_{CCN50}, SP_{CCN80}, and SP_{CCN100} values of 61%, 23%, and 14%, respectively (Fig. 4b). The SPs decreased by approximately 30% in the spring of 2007 and the fall of 2014. In 2017 and 2018, the average SP_{CCN50}, SP_{CCN80}, and SP_{CCN100} were only 10%, 4%, and 1%, respectively, indicating that only a minor fraction of new particles could grow to CCN sizes before being scavenged.

Figure 4c shows the percentage increase in the NPF-derived CCN relative to the pre-existing CCN. The percentages were the highest in the summer of 2014, e.g., 6.8×10^2%, 6.0×10^2%, and 4.8×10^2% for R_{CCN50}, R_{CCN80}, and R_{CCN100},

respectively. This finding could be attributed to the combination of high ΔN_{CCN} and low number concentrations of pre-existing particles in that campaign (Fig. S8-9). In the remaining four campaigns during 2007–2015, the percentages still exceeded 100%, i.e., 2.5×10^2%–3.8×10^2% for R_{CCN50}, 1.5×10^2%–2.9×10^2% for R_{CCN80}, and 1.1×10^2%–2.8×10^2% for R_{CCN100}. These ratios are within the range reported in the literature (50%–1.1×10^3%), although the calculation methods of the studies were slightly different (Lee et al., 2019). However, in 2017 and 2018, the percentages decreased considerably, e.g., <40% for R_{CCN50} and <20% for R_{CCN80} and R_{CCN100}.

4. Discussion

4.1 Question 1: What caused the unexpected responses of NPF to decreasing SO_2 concentrations?

H_2SO_4 oxidized from ambient SO_2 is one of the most important precursors for atmospheric nucleation. Decreases in ambient SO_2 mixing ratios, e.g., an annual average concentration decreases from 9 ppb to 1 ppb in Pittsburgh, 5 ppb to 3 ppb in Rochester, and 5 ppb to 2 ppb in Melpitz, have been reported to cause 40%–60% reductions in the NPF occurrence frequency and 40%–70% reductions in the NPF intensity (e.g., Hamed et al., 2010; Wang et al., 2011, 2017; Saha et al., 2018). However, this was not the case at the summit of Mt. Tai, where the NPF occurrence frequencies were almost invariant in the spring of 2007, summer of 2009, winter of 2017, and spring of 2018. The observed SO_2 mixing ratios in this study decreased considerably, from 15 ± 13 ppb in 2007 to 1.6 ± 1.6 ppb in 2018 (the SO_2 during the NPF periods decreased from 17 ± 11 ppb to 2.8 ± 1.8 ppb, Fig. 5a). In addition, the SO_2 emissions in China were reduced by approximately two-thirds from 2007 to 2018 (Fig. S1), where the sharpest reduction occurred in 2015–2016 owing to stringent mitigation policies.

As the calculated CSs before the NPF events in the 2017 and 2018 campaigns were higher than those in the 2007 and 2009 campaigns (Fig. 5b), CSs were unlikely to be the cause for the lack of decreases in the NPF occurrence frequency in 2017 and 2018. It has been reported that a low CS is not necessary to promote NPF occurrence at altitudes higher than 1000 m (Sellegri et al., 2019). Thus, other factors such as meteorological conditions and biogenic precursors (e.g., amines and highly oxidized organics) may overwhelm the effects of SO_2 and CS on the NPF occurrence frequency at Mt. Tai.

We further conducted a few statistical tests to explore the association of the apparent FR and NMINP with SO_2. The correlation analysis using the campaign averages showed weak negative correlations for the apparent FRs and NMINPs with the SO_2 mixing ratios ($r = 0.4$ and 0.3, respectively; both $p > 0.05$). Again, these results implied that other factors overwhelmed the effect of the SO_2 mixing ratios on the apparent FRs and NMINPs. When the observations were analyzed case by case, the correlations of the apparent FRs and NMINPs with the SO_2 mixing ratios were even weaker, with $r = -0.12$ and −0.14, respectively (both $p > 0.05$). Similar results were found when the estimated H_2SO_4 vapor was used for correlation analysis ($r = -0.12$ and −0.13, respectively; both $p > 0.05$). The scatter plots are shown in Fig. S10.

Recall that the occurrence frequencies of NPF were also almost the same in the spring of 2007 and 2018, at high values of 50-51%, implying that ambient factors in both campaigns favored NPF. Table 2 provides a comprehensive comparison of

the measured air pollutants of the two spring campaigns. The decrease in the SO_2, estimated H_2SO_4 concentration, and NH_3 did not explain the increases in the FRs and NMINP in 2018. Although amines were not measured, they are usually highly correlated with NH_3 (Xie et al., 2018). Based on the unique roles of HOMs in enhancing atmospheric nucleation and promoting the growth of new particles (Paasonen et al., 2010; Ehn et al., 2014; Kerminen et al., 2018), it was speculated that HOMs played an important role in the unexpected responses of NPF to lower SO_2 in 2018. Increased HOMs were expected on the NPF event days on the basis of the rapid afforestation over the last decade in China (Wang et a., 2020) and the increase in the forest areas surrounding the sampling site (Fig. S2). However, we had no measurements of HOMs. Nevertheless, the correlation between the FR and NMINP at Mt. Tai appears to support the hypothesis as presented below.

During the 106 cases of NPF events, the apparent FR and NMINP showed a good linear correlation ($r = 0.84$, $p < 0.01$) (Fig. 6). The fitted equation was highly consistent with those derived for urban and marine atmospheres (Man et al., 2015; Zhu et al., 2017, 2019; Ma et al., 2020). The strong linear relationship between the apparent FR and NMINP suggested that H_2SO_4 vapor was sufficient for nucleation, and the NPF intensity was very likely determined by the abundance of organic vapors available for participating in nucleation. Following the equation in the literature, i.e., $FR = k_{NucOrg}[H_2SO_4]^m [NucOrg]^n$ (where k_{NucOrg} is a constant, and m and n are integers; Zhang et al., 2012), the apparent FR is controlled by the concentrations of both H_2SO_4 vapor and organic vapor. We then considered two technical terms, i.e., the total concentration of H_2SO_4 vapor and the consumed amount of H_2SO_4 vapor for NPF. Unlike the apparent FR, the NMINP was always determined by the consumed amount of H_2SO_4 vapor, which may or may not have a positive correlation with the total concentration of H_2SO_4 vapor. The linear correlation between the FR and NMIMP suggests one possibility, i.e., the H_2SO_4 vapor was sufficient and the availability of organic vapor determined both the FR and the consumed amount of H_2SO_4 vapor proportional to the NMINP. Previous field measurements have shown that gaseous H_2SO_4 at concentrations of 10^5 molecules/cm^3 is necessary for NPF (McMurry et al., 2005; Nieminen et al., 2009; Erupe et al., 2010; Lee et al., 2019). In this study, the estimated H_2SO_4 concentration was in the range of 10^6–10^7 molecules/cm^3 and was theoretically sufficient for NPF (Table 2). Under other conditions, poor correlations are expected between the FR and NMIMP, e.g., with FR > 8 cm^{-3} s^{-1} reported in previous studies (open markers in Fig. 6).

Previous studies have reported that the BVOC emissions over the NCP have substantially increased in the last decade because of rapid afforestation and accelerating global warming (Stavrakou et al., 2014; Ma et al., 2019). During our observations, the TVOC (including C_2–C_{10}) mixing ratios approached 16.1 ± 6.5 ppb in the 2018 spring campaign, which was almost double that (including C_4–C_{12}) in the June 2006 campaign (Mao et al., 2009; no data from the spring 2007 campaign were available). The difference was highly consistent with the large increase in forest area over the last decade across the whole China. However, a large knowledge gap between the increase in BVOC emissions and the increase in nucleating organics still exists because of a lack of studies. Thus, the unexpected response of NPF events to reduced SO_2 still unexplained, and more measurements of H_2SO_4 and organics (e.g., HOMs) are needed. Note that the campaign average $PM_{2.5}$ mass concentration in 2018 indeed decreased. The decrease was apparently determined by the decrease in >153 nm

particles, since no significant difference existed in the calculated CS based on <153 nm particles between 2007 ($0.32 \pm 0.19\times10^{-2}$ s^{-1}) and 2018 ($0.40\pm0.15\times10^{-2}$ s^{-1}) .

4.2 Question 2: Did the contribution of NPF events to the CCN population decrease considerably with decreasing SO_2?

Based on the observations alone, the D_{pgmax} and the contribution of NPF to the CCN population decreased considerably with decreasing SO_2. However, the growth behaviors of new particles after the new particle signals disappeared from the observations were unknown. Thus, we further analyzed the D_{pgmax} in terms of the correlations with the calculated particle GR, the observation duration of the NPF events on site, and the underlying atmospheric processes.

Theoretically, the D_{pgmax} should be a function of the GR and the NPF duration. The GR is determined by real-time concentrations of condensation vapors, whereas the D_{pgmax} is determined by the availability of condensation vapor over a certain long period, both of which are influenced by the concentration of oxidants (Zhang et al., 2012, Apsokardu and Johnston, 2018). In this study, a moderate correlation was observed between D_{pgmax} and GR ($r = 0.58$, $p < 0.01$). The low r value suggested that the GR alone does not determine the D_{pgmax}. When one outlier was removed, r increased to 0.66 (Fig. 7a). In addition, the GR had a positive correlation with the total oxidant ($O_x = NO_2 + O_3$) but with an r as low as 0.38 ($p < 0.01$) (Fig. S11). Additionally, the D_{pgmax} and the duration of NPF events also showed good correlation ($r = 0.67$, $p < 0.01$) (Fig. 7e). Our results imply that both the real-time concentrations and the continuous supply of condensation vapor play dominant roles in the growth of new particles to the CCN size.

In further analysis, we considered three situations of the new particle growth. Type A (full marker in Fig. 7) represents that new particles continuously grow to the size of D_{pgmax} until the new particle signal drops to a negligible level. Type B (empty marker) represents the NPF events in which the growth of new particles is similar to that in Type A before D_{pgmax} is reached. After D_{pgmax} is reached, the grown new particles in Type B can still be observed for one more hour, after which either the growth stops for over one hour or the particles start shrinking to a smaller size until the new particle signal disappears. Type C (half-full marker) represents the NPF events that are not subject to Type A or B. Multistage growth of new particles can be observed for Type C particles. A few examples of the three types are shown in Fig. S12. We also separated the observations in 2017 and 2018 (in red) from those in 2007–2015 (in blue).

For Type A, the average GR and D_{pgmax} in 2017–2018 were only 1.5 nm h^{-1} and 23 nm, respectively, significantly lower than the 3.5 nm h^{-1} and 48 nm values observed in 2007–2015 ($p < 0.01$). When the regression equation of the GR and D_{pgmax} is examined, i.e., $D_{pgmax} = 11.0\times GR+8.2$ with a moderate good r, newly formed particles appear to grow beyond 50 nm only when the GR exceeds 3.8 nm h^{-1} in Type A. There was no significant difference between the duration of NPF events in 2017–2018 and that in 2007–2015. However, based on the regression equations between the duration and D_{pgmax} obtained in 2007–2015 and 2017–2018, newly formed particles could grow beyond 50 nm only when the NPF duration exceeded 9.9 h in 2007–2015, but the duration in 2017-2018 had to exceed 27.8 h. As reported in the literature, the lifetime of 50 nm

particles in the boundary layer is approximately one day, while that in the free troposphere is much longer (Williams et al., 2002). It can be argued that the new particles in Type A of 2007–2015 may still have been able to grow to the CCN size even after the new particle signal disappeared from the observation. However, the lifetime of 20 nm particles in the boundary layer is only several hours (Williams et al., 2002). If the Type A NPF events in 2017–2018 occurred in the boundary layer, the new particles may not have been able to grow to the CCN size before being scavenged from the ambient air. If they occurred in the free troposphere, the longer lifetime may have allowed the new particles in some events to be able to grow to the CCN size. For example, the NPF event on March 21, 2018 ended with an increase in the wind speed and a change in the wind direction, and the number concentration of new particles remained at a high level. The air mass back trajectories passed through the NCP at a high altitude (>1700 m a.g.l) at the beginning and end of the NPF event (Fig. S12a, b). In addition, the spikes of PNSDs during this NPF event indicated the vertical transport of atmospheric particles (Meng et al., 2015). We inferred that this NPF event seemingly occurred in the free troposphere, and a large decrease in the entrainment from the free troposphere to the boundary layer may have led to the disappearance of the new particle signal. Recent aircraft and airship measurements in northern and eastern China suggested that NPF events sometimes occurred in the free troposphere and then mixed down to the boundary layer (Quan et al., 2017; Qi et al., 2019).

In the case of Type B, the GR and D_{pgmax} in 2017–2018 (the mean values of 3.2 nm h^{-1} and 29 nm, respectively) were significantly lower than those in 2007–2015 (6.1 nm h^{-1} and 56 nm, respectively; $p < 0.01$). Following the regression equation of D_{pgmax} against GR, newly formed particles in Type B could grow beyond 50 nm only when the GR exceeded 5.8 nm h^{-1}. The number concentrations or the sizes of new particles decreased considerably at the end of Type B NPF events, and the transient time for the decrease suggested that the events occurred in the boundary layer. For example, the air mass back trajectories at the end of the NPF on April 7, 2018 originated from low altitude, and the height varied greatly over time (Fig. S12c, d). Most of the Type B NPF events in 2017–2018 may have had less opportunity to contribute to the CCN population, if they indeed occurred in the boundary layer. However, aircraft measurements are needed to confirm the altitude at which the NPF events occur. In addition, the changed boundary layer height had no detectable influence on D_{pgmax} as shown in Fig S13. However, the change in the late afternoon may largely decrease the observed number concentrations of grown new particles.

Type C was characterized by the largest GR, duration, and D_{pgmax}, with mean values of 7.7 nm h^{-1}, 22 h, and 92 nm, respectively. These particles underwent multiple growth processes, complicating the correlation between GR and D_{pgmax}, and that between duration and D_{pgmax}. The air mass back trajectories at the end of the NPF event on September 30, 2014 were local and originated at a low altitude (Fig. S12e, f), implying that these new particles experienced sufficient growth within the boundary layer. There were 16 Type C NPF events during 2007–2015 and only two in 2017. The lack of Type C NPF events in 2017–2018 implies a significant decrease in the contribution of new particles to the CCN population.

The factors influencing the lower D_{pgmax} and NPF-derived CCN population in 2017–2018 were further explored. In the literature, the growth of newly formed particles is mainly attributed to sulfuric acid, ammonium nitrate, and secondary

organic compounds (Wiedensohler et al., 2009; Riipinen et al., 2011; Zhang et al., 2012; Ehn et al., 2014; Man et al., 2015; Wang et al., 2015; Burkart et al., 2017; Lee et al., 2019; Wang et al., 2020). As listed in Table 2, the contribution of H_2SO_4 vapor to particle growth decreased from 36% in the spring of 2007 to 11% in the spring of 2018, indicating an inevitable consequence of decreasing SO_2 emission on particle growth. However, this percentage is likely not high enough to explain the 50% decrease in the GR and D_{pgmax} of Types A and B. On the other hand, the reduction in SO_2 and sulfate may reduce the aerosol acidity, subsequently affecting the acid-enhanced uptake of semivolatile organic species (Ding et al., 2011; Stangl et al., 2019). This hypothesis is supported by the lower level of organic carbon (OC) in $PM_{2.5}$ found in the spring of 2018 (5.5 ± 2.0 μg m^{-3}) than that in the spring of 2007 (6.1 ± 3.0 μg m^{-3}), although the BVOC emissions over the NCP have substantially increased in recent years (Table 2, Wang et al., 2011; Stavrakou et al., 2014; Ma et al., 2019; Dong et al., 2020). Furthermore, the mass concentration of nitrate in $PM_{2.5}$ was 7.4 ± 4.8 μg m^{-3} in 2007 during the new particle growth period, and it slightly decreased to 6.7± 5.5 μg m^{-3} in 2018. The reduced nitrate may also be partially responsible for the lack of Type C in 2018. In summary, we argued that the reduced H_2SO_4 vapor, nitrate and OC formation (most likely because of reduced anthropogenic emissions) may have led to the SP of new particles in the spring campaign of 2018 being lower than that of 2007. Unfortunately, chemical data about size-segregated molecular constituents are not available to confirm this finding, and therefore, more refined observations are urgently needed in the future.

However, uncertainties still exist, e.g., 1) the data were obtained in seven independent campaigns, each lasting in 18~71 days, and the data size did not allow us to extend the conclusion to all the years from 2007 to 2018; 2) the observations were conducted only at one site, alternating between the boundary layer and the free troposphere, and the generality of the conclusions on NPF events needs to be examined at more sites.

5. Conclusions

With an order of magnitude reduction in SO_2 emissions, the NPF frequency observed at the summit of Mt. Tai remained relatively constant during the seven campaigns of 2007–2018. The calculated campaign-based FR and NMINP were 0.8–1.2 cm^{-3} s^{-1} and 3.8–5.1 × 10^3 cm^{-3} in 2007–2014 and then unexpectedly increased by a factor of 2–3 in 2017–2018 to 2.0–3.0 cm^{-3} s^{-1} and 0.9–1.1 × 10^4 cm^{-3}, respectively. However, the large increase in the NPF intensity was accompanied by a smaller probability of the particles growing to the CCN size. The number concentrations of NPF-derived CCN with the three threshold sizes of 50, 80, and 100 nm were estimated to be 3.7×10^3, 1.6×10^3, and 8.6×10^2 cm^{-3} in the 2007 - 2015 campaigns, which then decreased to 1.0×10^3, 4.6×10^2, and 1.8×10^2 cm^{-3}, respectively, in the 2017 - 2018 campaigns. When the three types of NPF events are separately considered, it remains uncertain whether the new particles in Type A can grow to the CCN size after the disappearance of the new particle signals from observations. No conclusion can be drawn on this issue based on the current limited chemical observations. However, the new particles in Type B may have less opportunity to grow to the CCN size before they are scavenged from the ambient air. The lack of Type C NPF events in the campaigns of 2017–2018 indicates a large decrease in the probability of new particles growing to the CCN size with the reduction in ambient air

pollutants. Moreover, the shorter durations of the NPF events in the campaigns of 2017–2018 imply that the events occurred over a smaller spatial scale.

We hypothesize that the NPF intensity increased unexpectedly with the reduction in SO_2 concentration, as the net production of NPF seems to be determined mainly by the availability of organic precursors for participating in nucleation and initial growth. This is highly consistent with the large increase in forest areas over the last decade across China through rapid afforestation. The strong correlation between the FR and NMINP strongly supports this hypothesis, which needs to be further confirmed by direct observations of molecular organic vapors. The decrease in the percentage of new particles growing to the CCN size with increasing NPF intensity in 2017–2018 implies the complexity of the growth of new particles with reduced emissions of anthropogenic precursors under a large-scale increase in BVOC emissions. Overall, this study provides unique observational results regarding NPF at a regional mountain-top site in the NCP from reasonably large datasets. Based on the unique results, we comprehensively analyzed the possible causes, and proposed new challenges in determining the underlying mechanisms of the contributions of new particles to ambient particle number loading and CCN populations with reduced anthropogenic emissions.

Data availability. The datasets related to this work can be accessed via https://data.mendeley.com/datasets/wf3wjvpfw7/draft?a=adc7fab3-93b4-4f23-a075-904fe9729cf6.

Author contributions. LX designed the research. JC and JG conducted the field observations in 2007, 2014 and 2015. XW, HL, YZ, ZG, TC, LW, PZ, and YS carried out the field measurements in 2009, 2017 and 2018. YZ analyzed the data and wrote the paper. XY, TW and WW helped to interpretation of the results. XY and LX revised the original manuscript. All authors contributed toward improving the paper.

Competing interests. The authors declare that they have no conflict of interest.

Acknowledgements

This work was funded by the National Key Research and Development Program of China (2016YFC0200500), the National Natural Science Foundation of China (41922051, 42075104, 41706122), Shandong Provincial Science Foundation for Distinguished Young Scholars (ZR2019JQ09), and the Jiangsu Collaborative Innovation Center for Climate Change. We appreciate the NOAA Air Resource Laboratory for providing the HYSPLIT model, and thank the staff of the Mt. Tai Meteorological Station for the help during the measurement campaigns.

References

Apsokardu, M. J., and Johnston, M. V.: Nanoparticle growth by particle-phase chemistry, Atmos. Chem. Phys., 18, 1895–1907, https://doi.org/10.5194/acp-18-1895-2018, 2018.

Asmi, E., Kivekäs, N., Kerminen, V.-M., Komppula, M., Hyvärinen, A.-P., Hatakka, J., Viisanen, Y., and Lihavainen, H.: Secondary new particle formation in Northern Finland Pallas site between the years 2000 and 2010, Atmos. Chem. Phys., 11, 12959–12972, https://doi.org/10.5194/acp-11-12959-2011, 2011.

Charlson, R. J., Schwartz, S. E., Hales, J. M., Cess, R. D., Coakley, J. A., Hansen, J. E., and Hofmann, D. J.: Climate Forcing by Anthropogenic Aerosols. Science, 255, 423-430, 1992.

Chu, B., Kerminen, V. M., Bianchi, F., Yan, C., Petäjä, T., and Kulmala, M.: Atmospheric new particle formation in China. Atmos. Chem. Phys., 19, 115-138, https://doi.org/10.5194/acp-19-115-2019, 2019.

Dal Maso, M., Kulmala, M., Riipinen, I., Wagner, R., Hussein, T., Aalto, P. P., and Lehtinen, K. E. J.: Formation and growth of fresh atmospheric aerosols: Eight years of aerosol size distribution data from SMEAR II, Hyytiala, Finland, Boreal Environ. Res., 10, 323–336, 2005.

Ding, X., Wang, X., and Zheng, M.: The influence of temperature and aerosol acidity on biogenic secondary organic aerosol tracers: Observations at a rural site in the central Pearl River Delta region, South China, Atmos. Environ., 45, 1303-1311, https://doi.org/10.1016/j.atmosenv.2010.11.057, 2011.

Dong, S., Wang, X., Zhang J., Li, H., Li, W., Li, M., Gu, R., Jiang, Y., Shan, Y., Gao, X., Liu, H., Guo, Z., Xue, L., and Wang, W.: Light absorption properties, absorption contributions, and the influencing factors of atmospheric brown carbon on Mount Tai, Geochimica, 49, https://doi.org/10.19700/j.0379-1726.2020.01.011, 2020.

Dusek, U., Frank, G. P., Hildebrandt, L., Curtius, J., Schneider, J., Walter, S., Chand, D., Drewnick, F., Hings, S., Jung, D., Borrmann, S., and Andreae, M. O: Size matters more than chemistry for cloud-nucleating ability of aerosol particles, Science, 312, 1375–1378, https://doi.org/10.1126/science.1125261, 2006.

Ehn, M., Thornton, J. A., Kleist, E., Sipila, M., Junninen, H., Pullinen, I., Springer, M., Rubach, F., Tillmann, R., Lee, B., Lopez-Hilfiker, F., Andres, S., Acir, I.-H., Rissanen, M., Jokinen, T., Schobesberger, S., Kangasluoma, J., Kontkanen, J., Nieminen, T., Kurten, T., Nielsen, L. B., Jorgensen, S., Kjaergaard, H. G., Canagaratna, M., Dal Maso, M., Berndt, T., Petaja, T.,Wahner, A., Kerminen, V.-M., Kulmala, M.,Worsnop, D. R., Wildt, J., and Mentel, T. F.: A large source of lowvolatility secondary organic aerosol, Nature, 506, 476–479, https://doi.org/10.1038/nature13032, 2014.

Erupe, M. E., Benson, D. R., Li, J., Young, L. H., Verheggen, B., Al-Refai, M., Tahboub, O., Cunningham, V., Frimpong, F., Viggiano, A. A., and Lee, S. H.: Correlation of aerosol nucleation rate with sulfuricacid and ammonia in Kent, Ohio: An atmospheric observation, J. Geophys. Res. Atmos., 115, D23216, https://doi.org/10.1029/2010JD013942, 2010.

Fan, H., Zhao, C., and Yang, Y.: A comprehensive analysis of the spatio-temporal variation of urban air pollution in China during 2014–2018, Atmos. Environ., 220, 117066, https://doi.org/10.1016/j.atmosenv.2019.117066, 2020.

Gao, J.: Study on aerosol number concentration, size distribution and the particle formation and growth process, Doctoral dissertation, Jinan, Shandong University, 2008.

Gao, J., Wang, T., Ding, A. J. and Liu, C. B.: Observational Study of Ozone and Carbon Monoxide at the Summit of Mount Tai (1534 m a.s.l.) in Central eastern China, Atoms. Envrion., 39, 4779–4791, 2005.

Gao, J., Wang, T., Zhou, X., Wu, W., and Wang, W.: Measurement of aerosol number size distributions in the Yangtze River delta in China: Formation and growth of particles under polluted conditions, Atmos. Environ., 43, 829-836, 2009.

Guo, H., Wang, D. W., Cheung, K., Ling, Z. H., Chan, C. K., and Yao, X. H.: Observation of aerosol size distribution and new particle formation at a mountain site in subtropical Hong Kong, Atmos. Chem. Phys., https://doi.org/10.5194/acp-12-9923-2012, 2012.

Hamed, A., Birmili, W., Joutsensaari, J., Mikkonen, S., Asmi, A., Wehner, B., Spindler, G., Jaatinen, A., Wiedensohler, A., Korhonen, H., Lehtinen, K. E. J., and Laaksonen, A.: Changes in the production rate of secondary aerosol particles in Central Europe in view of decreasing SO_2 emissions between 1996 and 2006, Atmos. Chem. Phys., 10, 1071–1091, https://doi.org/10.5194/acp-10-1071-2010, 2010.

Hirsikko, A., Bergman, T., Laakso, L., Dal Maso, M., Riipinen, I., Hõrrak, U., and Kulmala, M.: Identification and classification of the formation of intermediate ions measured in boreal forest, Atmos. Chem. Phys., 7, 201–210, https://doi.org/10.5194/acp-7-201-2007, 2007.

Kalivitis, N., Kerminen, V.-M., Kouvarakis, G., Stavroulas, I., Tzitzikalaki, E., Kalkavouras, P., Daskalakis, N., Myriokefalitakis, S., Bougiatioti, A., Manninen, H. E., Roldin, P., Petäjä, T., Boy, M., Kulmala, M., Kanakidou, M., and Mihalopoulos, N.: Formation and growth of atmospheric nanoparticles in the eastern Mediterranean: results from long-term measurements and process simulations, Atmos. Chem. Phys., 19, 2671–2686, https://doi.org/10.5194/acp-19-2671-2019, 2019.

Kerminen, V. M., Chen, X., Vakkari, V., Petäjä, T., Kulmala, M., and Bianchi, F.: Atmospheric new particle formation and growth: review of field observations, Environ. Res. Lett., 13, 103003, https://doi.org/10.1088/1748-9326/Aadf3c, 2018.

Kerminen, V.-M., Paramonov, M., Anttila, T., Riipinen, I., Fountoukis, C., Korhonen, H., Asmi, E., Laakso, L., Lihavainen, H., Swietlicki, E., Svenningsson, B., Asmi, A., Pandis, S. N., Kulmala, M., and Petäjä, T.: Cloud condensation nuclei production associated with atmospheric nucleation: a synthesis based on existing literature and new results, Atmos. Chem. Phys., 12, 12037–12059, https://doi.org/10.5194/acp-12-12037-2012, 2012.

Krotkov, N. A., McLinden, C. A., Li, C., Lamsal, L. N., Celarier, E. A., Marchenko, S. V., Swartz, W. H., Bucsela, E. J., Joiner, J., Duncan, B. N., Boersma, K. F., Veefkind, J. P., Levelt, P. F., Fioletov, V. E., Dickerson, R. R., He, H., Lu, Z., and Streets, D. G.: Aura OMI observations of regional SO_2 and NO_2 pollution changes from 2005 to 2015, Atmos. Chem. Phys., 16, 4605–4629, https://doi.org/10.5194/acp-16-4605-2016, 2016.

Kulmala, M. and Kerminen, V. M.: On the formation and growth of atmospheric nanoparticles, Atmos. Res., 90, 132–150, https://doi.org/10.1016/j.atmosres.2008.01.005, 2008.

Kulmala, M., Dal Maso, M., Mäkelä, M., Pirjola, L., Väkevä, M., Aalto, P., Miikkulainen, P., and Hämeri, K.: On the formation, growth and composition of nucleation mode particles, Tellus B, 53, 479–490, https://doi.org/10.1034/j.1600-0889.2001.d01-33.x, 2001.

Kulmala, M., Petäjä, T., Nieminen, T., Sipilä, M., Manninen, H. E., Lehtipalo, K., Dao Maso, M., Aalto, P. P., Junninen, H., Paasonen, P., Riipinen, I., Lehtinen, K. E. J., Laaksonen, A., and Kerminen, V-M.: Measurement of the nucleation of atmospheric aerosol particles, Nat. Protoc., 7, 1651–1667, https://doi.org/10.1038/nprot.2012.091, 2012.

Kulmala, M., Vehkamäki, H., Petäjä, T., Dal Maso, M., Lauri, A., Kerminen, V.-M., Birmili, W., and McMurry, P. H.: Formation and growth rates of ultrafine atmospheric particles: a review of observations, J. Aerosol Sci., 35, 143–176, https://doi.org/10.1016/j.jaerosci.2003.10.003, 2004.

Lee, S., Gordon, H., Yu, H., Lehtipalo, K., Haley, R., Li, Y., and Zhang, R.: New particle formation in the atmosphere: From molecular clusters to global climate, J. Geophys. Res. Atmos., 124, 7098-7146, https://doi.org/10.1029/2018JD029356, 2019.

Li, H. Y., Zhu, Y. J., Zhao, Y., Chen, T. S., Jiang, Y., Shan, Y., Liu, Y. H., Mu, J. S., Yin, X. K., Wu, D., Zhang, C., Si, S. C., Wang, X. F., Wang, W. X., Xue, L. K. Evaluation of the Performance of Low-Cost Air Quality Sensors at a High Mountain Station with Complex Meteorological Conditions, Atmosphere, 11, 212; doi:10.3390/atmos11020212, 2020.

Li, K., Zhu, Y., Gao, H., and Yao, X.: A comparative study of cloud condensation nuclei measured between non-heating and heating periods at a suburb site of Qingdao in the North China, Atmos. Environ., 112, 40-53, https://doi.org/10.1016/j.atmosenv.2015.04.024, 2015.

Li, W. J., Zhang, D. Z., Shao, L. Y., Zhou, S. Z., and Wang, W. X.: Individual particle analysis of aerosols collected under haze and non-haze conditions at a high-elevation mountain site in the North China plain, Atmos. Chem. Phys., 11, 11733-11744, http://dx.doi.org/ 10.5194/acp-11-11733-2011, 2011.

Li, X., Zhao, B., Zhou, W., Shi, H., Yin, R., Cai, R., Yang, D., Dällenbach, K., Deng, C., Fu, Y., Qiao, X., Wang, L., Liu, Y., Yan, C., Kulmala, M., Zheng, J., Hao, J., Wang, S., and Jiang, J.: Responses of gaseous sulfuric acid and particulate sulfate to reduced SO2 concentration: A perspective from long-term measurements in Beijing, Sci. Total Environ., 137700, https://doi.org/10.1016/j.scitotenv.2020.137700, 2020.

Lihavainen, H., Kerminen, V.-M., Komppula, M., Hatakka, J., Aaltonen, V., Kulmala, M., and Viisanen, Y.: Production of "potential" cloud condensation nuclei associated with atmospheric newparticle formation in northern Finland, J. Geophys. Res.-Atmos., 108, 4782, doi:10.1029/2003JD003887, 2003.

Lv, G., Sui, X., Chen, J., Jayaratne, R., and Mellouki, A.: Investigation of new particle formation at the summit of Mt. Tai, China, Atmos. Chem. Phys., 18, 2243–2258, https://doi.org/10.5194/acp-18-2243-2018, 2018.

Ma, L., Zhu, Y., Zheng, M., Sun, Y., Huang, L., Liu, X., Gao, Y., Shen, Y., Gao, H., and Yao, X.: Investigating three patterns of new particles growing to cloud condensation nuclei size in Beijing's urban atmosphere, Atmos. Chem. Phys. Diss., 2020.

Ma, M., Gao, Y., Wang, Y., Zhang, S., Leung, L. R., Liu, C., Wang, S., Zhao, B., Chang, X., Su, H., Zhang, T., Sheng, L., Yao, X., and Gao, H.: Substantial ozone enhancement over the North China Plain from increased biogenic emissions due to heat waves and land cover in summer 2017, Atmos. Chem. Phys., 19, 12195–12207, https://doi.org/10.5194/acp-19-12195-2019, 2019.

Ma, N., Zhao, C., Tao, J., Wu, Z., Kecorius, S., Wang, Z., Größ, J., Liu, H., Bian, Y., Kuang, Y., Teich, M., Spindler, G., Müller, K., van Pinxteren, D., Herrmann, H., Hu, M., and Wiedensohler, A.: Variation of CCN activity during new particle formation events in the North China Plain, Atmos. Chem. Phys., 16, 8593–8607, https://doi.org/10.5194/acp-16-8593-2016, 2016.

Man, H., Zhu, Y., Ji, F., Yao, X., Lau, N. T., Li, Y. J., Lee, B. P., and Chan, C. K.: Comparison of daytime and nighttime new particle growth at the HKUST Supersite in Hong Kong, Environ. Sci. Technol., 49, 7170–7178, https://doi.org/10.1021/acs.est.5b02143, 2015.

Mao, T., Wang, Y., Xu, H., Jiang, J., Wu, F., and Xu, X.: A study of the atmospheric VOCs of Mount Tai in June 2006, Atoms. Envrion., 43, 2503-2508, https://doi.org/10.1016/j.atmosenv.2009.02.013, 2009.

McMurry, P. H., Fink, M., Sakurai, H., Stolzenburg, M. R., Mauldin, III R. L., Smith, J., Eisele, F., Moore, K., Sjostedt, S., Tanner, D., Huey, L. G., Nowak, J. B., Edgerton, E., and Voisin D.: A criterion for new particle formation in the sulfur-rich Atlanta atmosphere, J. Geophys. Res. Atmos., 110, D22S02. https://doi.org/10.1029/2005JD005901, 2005.

Meng, H., Zhu, Y. J., Evans, G., and Yao, X. H.: An approach to investigate new particle formation in the vertical direction on the basis of high time-resolution measurements at ground level and sea level, Atmos. Environ., 102, 366-375, https://doi.org/10.1016/j.atmosenv.2014.12.016, 2015.

Merikanto, J., Spracklen, D. V., Mann, G. W., Pickering, S. J., and Carslaw, K. S.: Impact of nucleation on global CCN, Atmos. Chem. Phys., 9, 8601–8616, https://doi.org/10.5194/acp-9-8601-2009, 2009.

Mikkonen, S., Romakkaniemi, S., Smith, J. N., Korhonen, H., Petäjä, T., Plass-Duelmer, C., Boy, M., McMurry, P. H., Lehtinen, K. E. J., Joutsensaari, J., Hamed, A., Mauldin III, R. L., Birmili, W., Spindler, G., Arnold, F., Kulmala, M., and Laaksonen, A.: A statistical proxy for sulphuric acid concentration, Atmos. Chem. Phys., 11, 11319-11334, https://doi.org/10.5194/acp-11-11319-2011, 2011.

Nie, W., Ding, A., Wang, T., Kerminen, V., George, C., Xue, L., Wang, W., Zhang, Q., Petaja, T., Qi, X., Gao, X., Wang, X., Yang, X., Fu, C., and Kulmala, M.: Polluted dust promotes new particle formation and growth, Sci. Rep., 4, 6634. https://doi.org/10.1038/srep06634, 2014

Nieminen, T., Asmi, A., Dal Maso, M., Aalto, P. P., Keronen, P., Petäjä, T., Kulmala, M., and Kerminen, V-M.: Trends in atmospheric new-particle formation: 16 years of observations in a boreal-forest environment, Boreal Environ. Res., 19 191-214, 2014.

Nieminen, T., Manninen, H. E., Sihto, S. L., Yli-Juuti, T., Mauldin, III R. L., Petäjä, T., Riipinen, I., Kerminen, V.-M., and Kulmala, M.: Connection of sulfuric acid to atmospheric nucleation in boreal forest, Environ. Sci. Technol., 43, 4715–4721. https://doi.org/10.1021/es803152j, 2009.

Paasonen, P., Nieminen, T., Asmi, E., Manninen, H. E., Petäjä, T., Plass-Dülmer, C., Flentje, H., Birmili, W., Wiedensohler, A., Hõrrak, U., Metzger, A., Hamed, A., Laaksonen, A., Facchini, M. C., Kerminen, V.-M., and Kulmala, M.: On the roles of sulphuric acid and low-volatility organic vapours in the initial steps of atmospheric new particle formation, Atmos. Chem. Phys., 10, 11223–11242, https://doi.org/10.5194/acp-10-11223-2010, 2010.

Petters, M. D., and Kreidenweis, S. M.: A single parameter representation of hygroscopic growth and cloud condensation nucleus activity, Atmos. Chem. Phys., 7, 1961–1971, https://doi.org/10.5194/acp-7-1961-2007, 2007.

Qi, X., Ding, A., Nie, W., Chi, X., Huang, X., Xu, Z., Wang, T., Wang, Z., Wang, J., Sun, P., Zhang, Q., Huo, J., Wang, D., Bian, Q., Zhou, L., Zhang, Q., Ning, Z., Fei, D., Xiu, G., and Fu, Q.: Direct measurement of new particle formation based on tethered airship around the top of the planetary boundary layer in eastern China, Atmos. Environ., 209, 92-101. https://doi.org/10.1016/j.atmosenv.2019.04.024, 2019.

Quan, J., Liu, Y., Liu, Q., Jia, X., Li, X., Gao, Y., Ding, D., and Wang, Z.: Anthropogenic pollution elevates the peak height of new particle formation from planetary boundary layer to lower free troposphere, Geophys. Res. Lett., 44, 7537-7543, https://doi.org/10.1002/2017GL074553, 2017.

Riipinen, I., Yli-Juuti, T., Pierce, J. R., Petäjä, T., Worsnop, D. R., Kulmala, M., and Donahue, N. M.: The contribution of organics to atmospheric nanoparticle growth, Nat. Geosci., 5, 453–458, https://doi.org/10.1038/ngeo1499, 2012.

Rose, C., Sellegri, K., Moreno, I., Velarde, F., Ramonet, M., Weinhold, K., Krejci, R., Andrade, M., Wiedensohler, A., Ginot, P., and Laj, P.: CCN production by new particle formation in the free troposphere, Atmos. Chem. Phys., 17, 1529-1541, https://doi.org/10.5194/acp-17-1529-2017, 2017.

Saha, P. K., Robinson, E. S., Shah, R. U., Zimmerman, N., Apte, J. S., Robinson, A. L., and Presto, A.: Reduced ultrafine particle concentration in urban air: changes in nucleation and anthropogenic emissions, Environ. Sci. Technol., 52, 6798–806, https://doi.org/10.1021/acs.est.8b00910, 2018.

Seinfeld, J.H. and Pandis, S.N.: Atmospheric chemistry and physics: From air pollution to climate change, John Wiley & Sons, New York, 2012.

Sellegri, K., Rose, C., Marinoni, A., Lupi, A., Wiedensohler, A., Andrade, M., Bonasoni, P., and Laj, P.: New Particle Formation: A Review of Ground-Based Observations at Mountain Research Stations, Atmosphere, 10, 493, https://doi.org/10.3390/atmos10090493, 2019.

Shen, L., Wang, H., Yin, Y., Chen, J., and Chen, K.: Observation of atmospheric new particle growth events at the summit of mountain Tai (1534 m) in Central East China, Atmos. Environ., 201, 148-157, https://doi.org/10.1016/j.atmosenv.2018.12.051, 2019.

Shen, X., Sun, J., Zhang, X., Kivekäs, N., Zhang, Y., Wang, T., Zhang, X., Yang, Y., Wang, D., Zhao, Y., and Qin, D.: Particle climatology in Central East China retrieved from measurements in planetary boundary layer and in free troposphere at a 1500-m-High mountaintop site, Aerosol Air Qual. Res, 16, 689-701, 2016a.

Shen, X. J., Sun, J. Y., Zhang, X. Y., Zhang, Y. M., Zhang, L., and Fan, R. X.: Key features of new particle formation events at background sites in China and their influence on cloud condensation nuclei, Fron. Environ. Sci. Eng., 10, 5, https://doi.org/10.1007/s11783-016-0833-2, 2016b.

Sihto, S.-L., Kulmala, M., Kerminen, V.-M., Dal Maso, M., Petäjä, T., Riipinen, I., Korhonen, H., Arnold, F., Janson, R., Boy, M., Laaksonen, A., and Lehtinen, K. E. J.: Atmospheric sulphuric acid and aerosol formation: implications from atmospheric measurements for nucleation and early growth mechanisms, Atmos. Chem. Phys., 6, 4079–4091, https://doi.org/10.5194/acp-6-4079-2006, 2006.

Stangl, C. M., Krasnomowitz, J. M., Apsokardu, M. J., Tiszenkel, L., Ouyang, Q., Lee, S., and Johnston, M. V.: Sulfur dioxide modifies aerosol particle formation and growth by ozonolysis of monoterpenes and isoprene, J. Geophys. Res. Atmos., 124(8), 4800-4811. https://doi.org/10.1029/2018JD030064, 2019.

Stavrakou, T., Müller, J.-F., Bauwens, M., De Smedt, I., Van Roozendael, M., Guenther, A., Wild, M., and Xia, X.: Isoprene emissions over Asia 1979–2012: impact of climate and land-use changes, Atmos. Chem. Phys., 14, 4587–4605, https://doi.org/10.5194/acp-14-4587-2014, 2014.

Sun, L., Xue, L., Wang, T., Gao, J., Ding, A., Cooper, O. R., Lin, M., Xu, P., Wang, Z., Wang, X., Wen, L., Zhu, Y., Chen, T., Yang, L., Wang, Y., Chen, J., and Wang, W., Significant increase of summertime ozone at Mount Tai in Central Eastern China, Atmos. Chem. Phys., 16, 10637–10650, https://doi.org/10.5194/acp-16-10637-2016, 2016.

Tröstl, J., Chuang, W. K., Gordon, H., Heinritzi, M., Yan, C., Molteni, U., Ahlm, L., Frege, C., Bianchi, F., Wagner, R., Simon, M., Lehtipalo, K., Williamson, C., Craven, J. S., Duplissy, J., Adamov, A., Almeida, J., Bernhammer, A.-K., Breitenlechner, M., Brilke, S., Dias, A., Ehrhart, S., Flagan, R. C., Franchin, A., Fuchs, C., Guida, R., Gysel, M., Hansel, A., Hoyle, C. R., Jokinen, T., Junninen, H., Kangasluoma, J., Keskinen, H., Kim, J., Krapf, M., Kuerten, A., Laaksonen, A., Lawler, M., Leiminger, M., Mathot, S., Moehler, O., Nieminen, T., Onnela, A., Petaejae, T., Piel, F. M., Miettinen, P., Rissanen, M. P., Rondo, L., Sarnela, N., Schobesberger, S., Sengupta, K., Sipila, M., Smith, J. N., Steiner, G., Tome, A., Virtanen, A., Wagner, A. C., Weingartner, E., Wimmer, D., Winkler, P. M., Ye, P., Carslaw, K. S., Curtius, J., Dommen, J., Kirkby, J., Kulmala, M., Riipinen, I., Worsnop, D. R., Donahue, N. M., and Baltensperger, U.: The role of low-volatility organic compounds in initial particle growth in the atmosphere, Nature, 533, 527–531, https://doi.org/10.1038/nature18271, 2016.

Wang, J., Feng, L., Palmer, P. I., Liu, Y., Fang, S., Bösch, H., O'Dell, C. W., Tang, X., Yang, D., Liu, L., and Xia, C. Z. Large Chinese land carbon sink estimated from atmospheric carbon dioxide data, Nature, 586, 720-723, https://doi.org/10.1038/s41586-020-2849-9, 2020.

Wang, Y., Hopke, P. K., Chalupa, D. C., and Utell, M. J.: Long-term study of urban ultrafine particles and other pollutants, Atmos. Environ., 45, 7672-7680, https://doi.org/10.1016/j.atmosenv.2010.08.022, 2011.

Wang, Z., Birmili, W., Hamed, A., Wehner, B., Spindler, G., Pei, X. ,Wu, Z., Cheng, Y., Su, H., and Wiedensohler, A.: Contributions of volatile and nonvolatile compounds (at 300 °C) to condensational growth of atmospheric nanoparticles: an assessment based on 8.5 years of observations at the central Europe background site Melpitz, J. Geophys. Res. Atmos., 122, 485–97, https://doi.org/10.1002/2016JD025581, 2017.

Wang, Z., Wang, T., Gao, R., Xue, L., Guo, J., Zhou, Y., Nie, W., Wang, X., Xu, P., Gao, J., Zhou, X., Wang, W., and Zhang, Q.: Source and variation of carbonaceous aerosols at Mount Tai, North China: Results from a semi-continuous instrument, Atoms. Envrion., 45, 1655-1667, https://doi.org/10.1016/j.atmosenv.2011.01.006, 2011.

Wen, L., Xue, L., Wang, X., Xu, C., Chen, T., Yang, L., Wang, T., Zhang, Q., and Wang, W.: Summertime fine particulate nitrate pollution in the North China Plain: increasing trends, formation mechanisms and implications for control policy, Atmos. Chem. Phys., 18, 11261–11275, https://doi.org/10.5194/acp-18-11261-2018, 2018.

Whitby, K. T.: The physical characteristics of sulfur aerosols, Atoms. Envrion., 12, 135-159, 1978.

Williams, J., de Reus, M., Krejci, R., Fischer, H., and Ström, J.: Application of the variability-size relationship to atmospheric aerosol studies: estimating aerosol lifetimes and ages, Atmos. Chem. Phys., 2, 133–145, https://doi.org/10.5194/acp-2-133-2002, 2002.

Wu, Z. J., Hu, M., Liu, S., Wehner, B., Bauer, S., Ssling, A. M., Wiedensohler, A., Petaja, T., Dal Maso, M., and Kulmala, M.: New particle formation in Beijing, China: Statistical analysis of a 1-year data set, J. Geophys. Res.-Atmos., 112, D09209, https://doi.org/10.1029/2006jd007406, 2007.

Xie., H., Feng, L., Hu, Q., Zhu, Y., Gao, H., Gao, Y., and Yao, X.: Concentration and size distribution of water-extracted dimethylaminium and trimethylaminium in atmospheric particles during nine campaigns - Implications for sources, phase states and formation pathways, Sci. Total Environ., 130–141, https://doi.org/10.1016/j.scitotenv.2018.02.303, 2018.

Yao, L., Garmash, O., Bianchi, F., Zheng, J., Yan, C., Kontkanen, J., Junninen, H., Mazon, S.B, Ehn, M., Paasonen, P., Sipilä, M., Wang, M., Wang, X., Xiao, S., Chen, H., Lu, Y., Zhang, B., Wang, D., Fu, Q., Geng, F., Li, L., Wang, H., Qiao, L., Yang, X., Chen, J., Kerminen, V. M., Petäjä, T., Worsnop, D. R., Kulmala, M., and Wang. L.: Atmospheric new particle formation from sulfuric acid and amines in a Chinese megacity, Science, 361, 278-281, https://doi.org/10.1126/science.aao4839, 2018.

Zhang, R., Khalizov, A., Wang, L., Hu, M., and Xu, W.: Nucleation and growth of nanoparticles in the atmosphere, Chem. Rev., 112, 1957–2011, https://doi.org/10.1021/cr2001756, 2012.

Zhou, Y., Wang, T., Gao, X., Xue, L., Wang, X., Wang, Z., Gao, J., Zhang Q., and Wang, W.: Continuous observations of water-soluble ions in $PM_{2.5}$ at Mount Tai (1534 m asl) in central-eastern China, J. Atmos. Chem., 64, 107-127, https://doi.org/10.1007/s10874-010-9172-z, 2009.

Zhu, Y., Li, K., Shen, Y., Gao, Y., Liu, X., Yu, Y., Gao, H., and Yao, X.: New particle formation in the marine atmosphere during seven cruise campaigns, Atmos. Chem. Phys., 19, 89–113, https://doi.org/10.5194/acp-19-89-2019, 2019.

Zhu, Y., Sabaliauskas, K., Liu, X., Meng, H., Gao, H., Jeong, C. H., Evans, G. J., and Yao, X.: Comparative analysis of new particle formation events in less and severely polluted urban atmosphere, Atmos. Environ., 98, 655–664, https://doi.org/10.1016/j.atmosenv.2014.09.043, 2014.

Zhu, Y., Yan, C., Zhang, R., Wang, Z., Zheng, M., Gao, H., Gao, Y., and Yao, X.: Simultaneous measurements of new particle formation at 1 s time resolution at a street site and a rooftop site, Atmos. Chem. Phys., 17, 9469–9484, https://doi.org/10.5194/acp-17-9469-2017, 2017.

Zhu, Y., Yang, L., Kawamura, K., Chen, J., Ono, K., Wang, X., Xue, L., and Wang, W.: Contributions and source identification of biogenic and anthropogenic hydrocarbons to secondary organic aerosols at Mt. Tai in 2014, Environ. Pollut., 220, 863-872, https://doi.org/10.1016/j.envpol.2016.10.070, 2017.

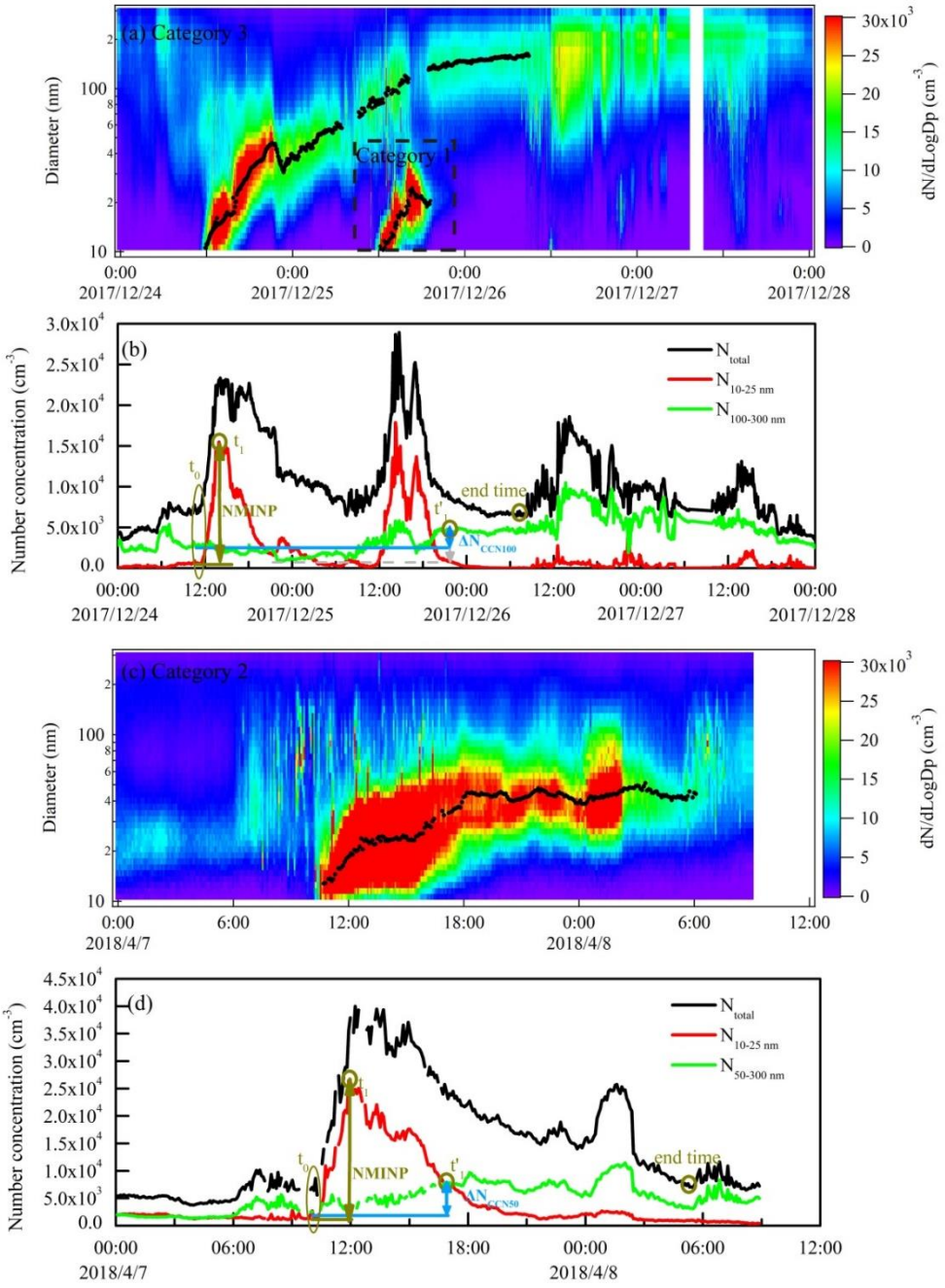

Figure 1: Examples of NPF events in three categories. Black dots in the figures are the fitted D_{pg}. (a) Category 1 on December 25, 2017, in which D_{pgmax} was 24 nm (<50 nm), and Category 3 on December 24, 2017, in which D_{pgmax} grew to 163 nm (>80 nm); (c) Category 2 on April 7, 2018, in which D_{pgmax} grew to 53 nm (50–80 nm). (b, d) Schematic diagram of t_0, t_1, t'_1, NMINP and ΔN_{CCN100}/ ΔN_{CCN50} on December 24, 2017 and April 7, 2018 NPF events (a few spikes have been removed from Figure d).

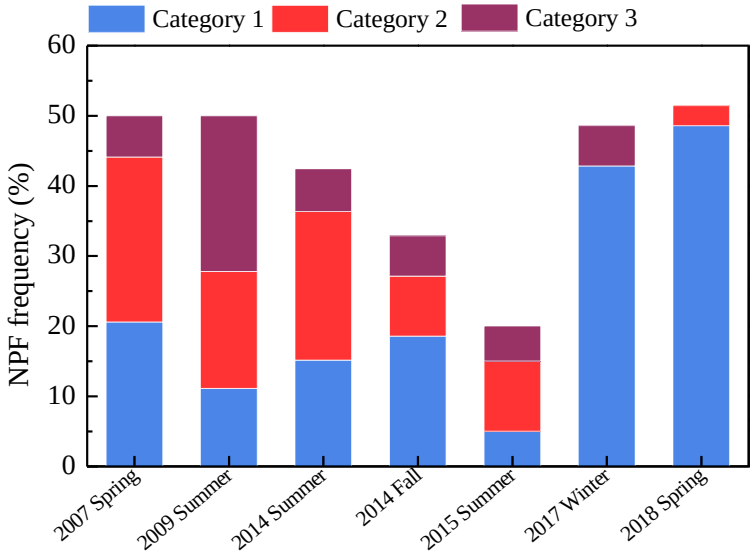

740

Figure 2: Occurrence frequencies of NPF events in different categories at Mt. Tai during the seven observation campaigns.

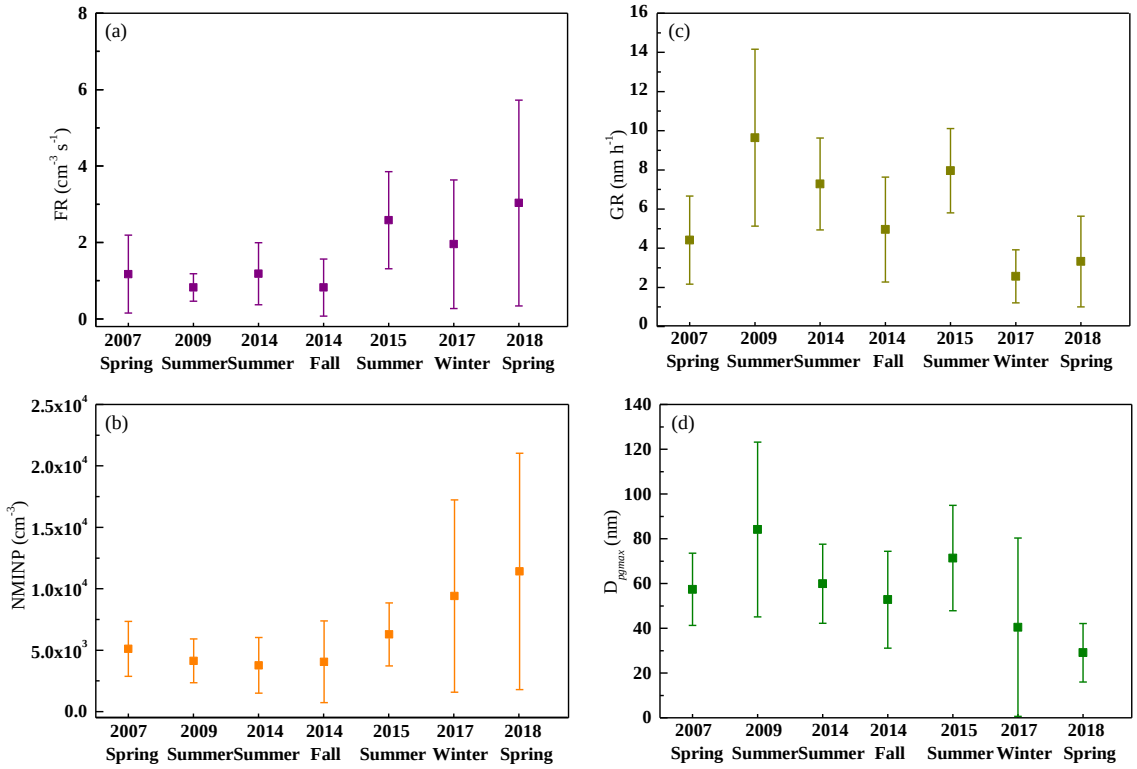

745

Figure 3: Campaign average of the new particle formation rate (FR, a), the net maximum increase in the nucleation-mode particle number concentration (NMINP, b), the new particle growth rate (GR, c), and the maximum geometric median diameter of the grown new particles (D_{pgmax}, d) during the seven observation campaigns. The error bars are the standard deviations.

750

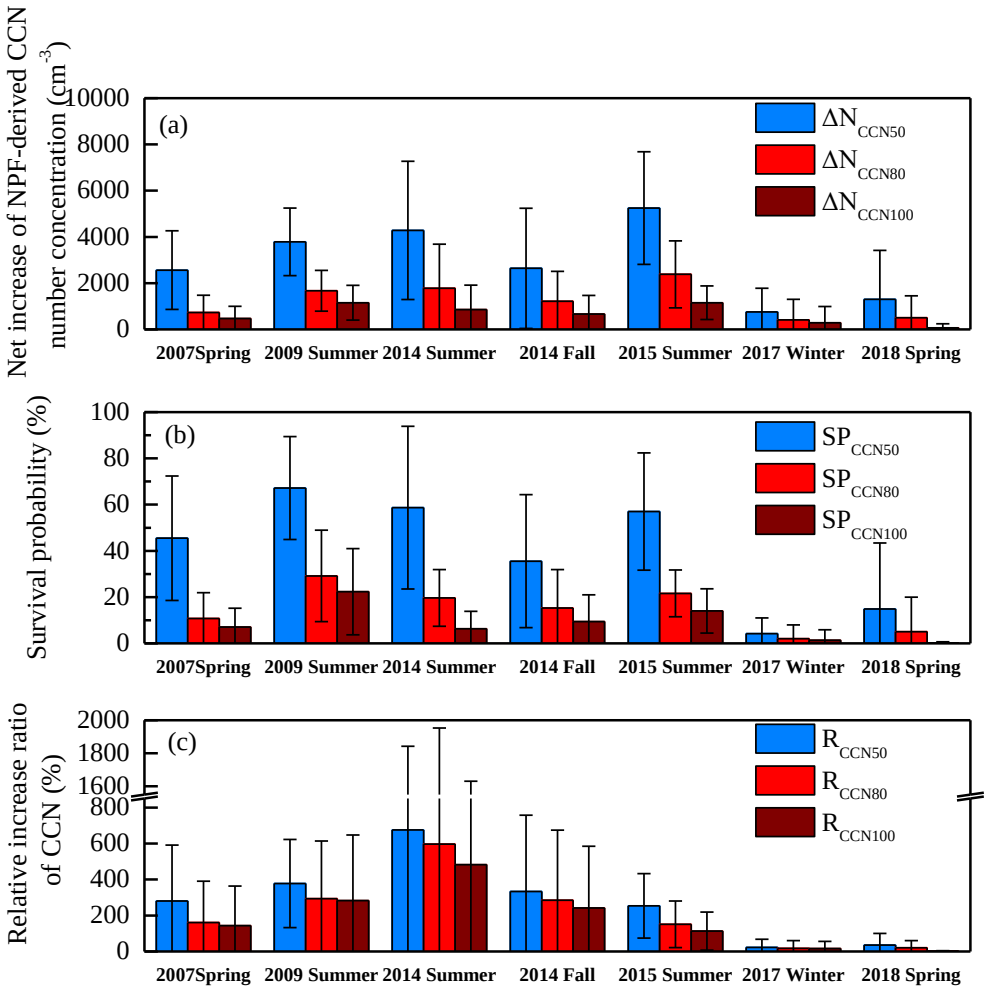

Figure 4: Campaign average of the net increase in the NPF-derived CCN number concentration (ΔN_{CCN}, a), the survival probability of new particles growing to CCN sizes (SP_{CCN}, b), and the relative increase ratio of the CCN population (R_{CCN}, c) during the seven observation campaigns. The error bars are the standard deviations.

755

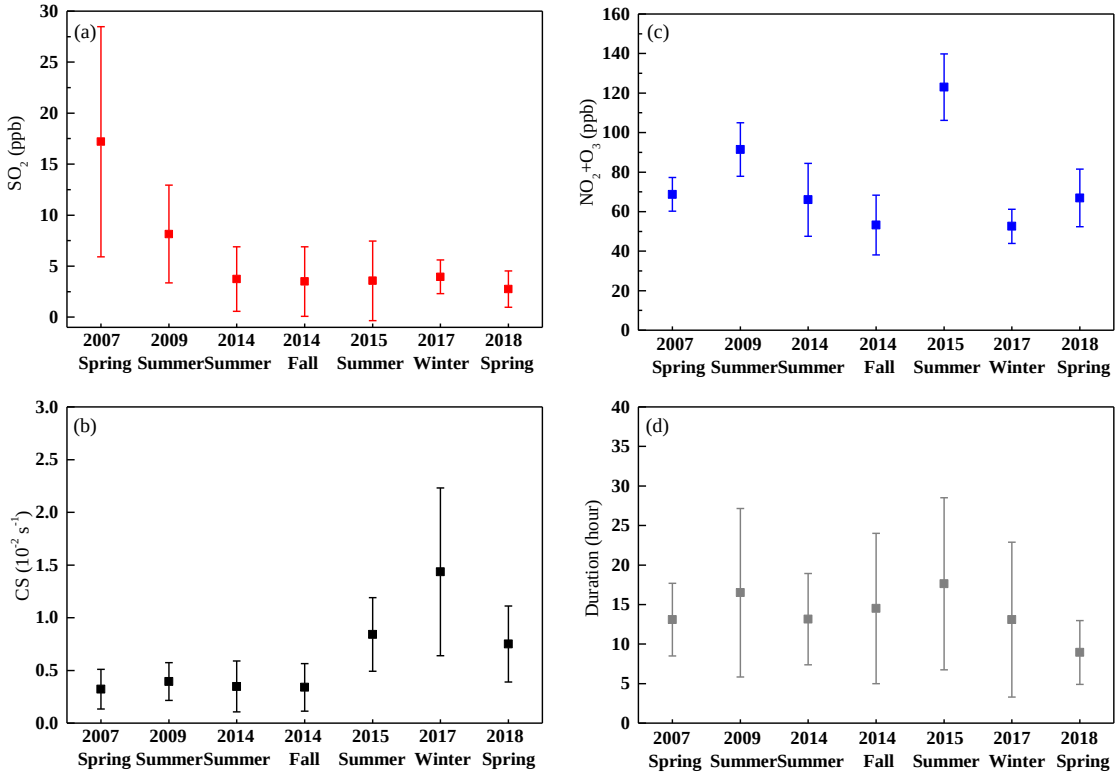

Figure 5: Campaign average of SO_2 mixing ratios (average during NPF periods, a), CS (one hour prior to NPF events, b), $NO_2 + O_3$ (average during new particle growth periods, c), and NPF event durations (d) during the seven observation campaigns. The error bars are the standard deviations.

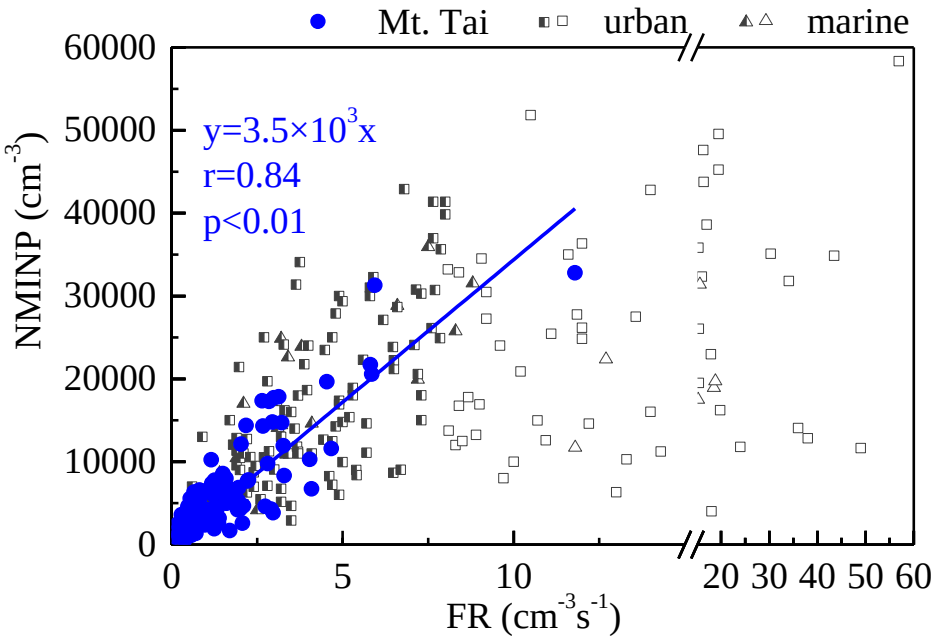

Figure 6: Relationship between the FR and NMINP in 106 cases of NPF events at Mt. Tai in this study and in urban and marine atmospheres in previous studies (Man et al., 2015; Zhu et al., 2017, 2019; Ma et al., 2020). The half-solid markers can be fitted linearly in previous studies. The open markers show poor correlations.

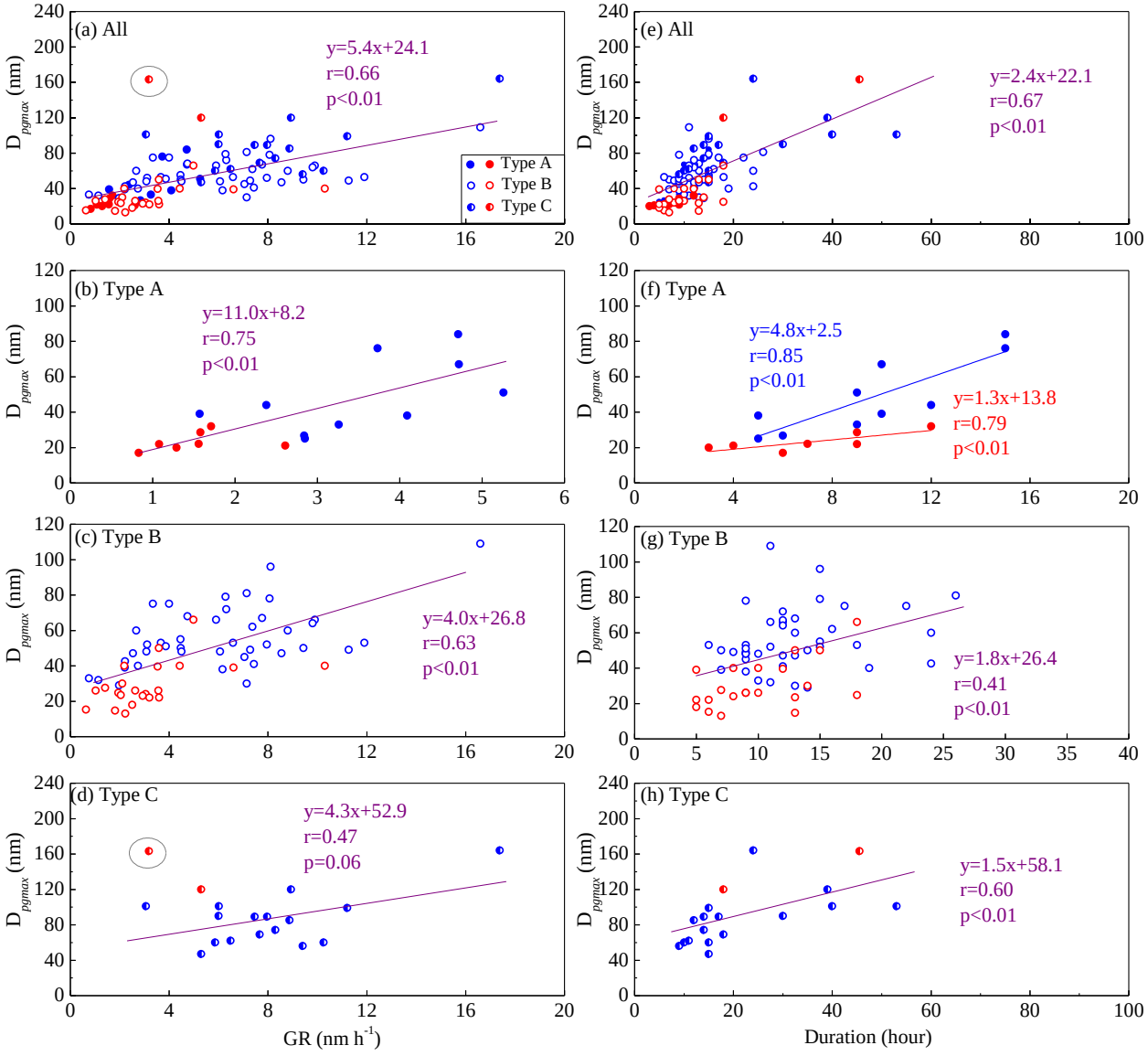

Figure 7: Relationship between the GR and D_{pgmax} (a–d) and between the duration of NPF events and D_{pgmax} (e–h). Solid marker represents Type A; empty marker represents Type B; and half-solid marker represents Type C. Red markers and equations represent 2017 and 2018, and blue markers and equations represent 2007–2015. The purple equation represents fitting of all data, and the circled marker represents an outlier from the equation fit.

Table 1. Summary of the seven observation campaigns at Mt. Tai.

Campaign	Species	Instruments	Resolution
Spring 2007 3/22–4/24, 2007	PNSD in 10 nm–10 μm	WPS, MSP 1000XP	8 min
	SO_2, O_3, NO, and NO_2	Thermo 43C, 49C, 42C	1 min
	$PM_{2.5}$	TEOM 1400a	1 min
	Water-soluble ions in $PM_{2.5}$	URG-AIM 9000B	1 h
Summer 2009 6/12–6/29, 2009	PNSD in 10 nm–10 μm	WPS, MSP 1000XP	8 min
	SO_2, O_3, NO, and NO_2	Thermo 43C, 49C, 42C	1 min
Summer 2014 7/26–8/27, 2014	PNSD in 5 nm–10 μm	WPS, MSP 1000XP	5 min
	SO_2, O_3, NO, and NO_2	Thermo 43C, 49C,42i	1 min
	$PM_{2.5}$	Thermo 5030 SHARP	1 min
	Ions in $PM_{2.5}$, acid, and alkaline gases	MARGA, ADI20801	1 h
Fall 2014 9/21–11/30, 2014	PNSD in 5 nm–10 μm	WPS, MSP 1000XP	5 min
	SO_2, O_3	Thermo 43C, 49C	1 min
	NO, NO_2	API T200U, T500U	1 min
	$PM_{2.5}$	Thermo 5030 SHARP	1 min
	Ions in $PM_{2.5}$, acid, and alkaline gases	MARGA, ADI20801	1 h
Summer 2015 6/16–7/25, 2015	PNSD in 5 nm–10 μm	WPS, MSP 1000XP	5 min
	SO_2, O_3	Thermo 43C,49C	1 min
	NO, NO_2	API T200U, T500U	1 min
	$PM_{2.5}$	Thermo 5030 SHARP	1 min
	Ions in $PM_{2.5}$, acid, and alkaline gases	MARGA, ADI20801	1 h
Winter 2017 11/26–12/30, 2017	PNSD in 5 nm–10 μm	WPS, MSP 1000XP	5 min
	SO_2, O_3	Thermo 43C, API 400U	1 min
	NO, NO_2	API T200U, T500U	1 min
	$PM_{2.5}$	Thermo 5030 SHARP	1 min
	Ions in $PM_{2.5}$, acid, and alkaline gases	MARGA, ADI20801	1 h
Spring 2018 3/5–4/8, 2018	PNSD in 5 nm–10 μm	WPS, MSP 1000XP	5 min
	SO_2, O_3	Thermo 43C, API 400U	1 min
	NO, NO_2	API T200U, T500U	1 min
	$PM_{2.5}$	Thermo 5030 SHARP	1 min
	Ions in $PM_{2.5}$, acid, and alkaline gases	MARGA, ADI20801	1 h

Table 2. Meteorological conditions and air pollutants during the formation and growth periods of new particles in the spring campaigns in 2007 and 2018.

Parameters	2007 spring		2018 spring	
	Formation	Growth	Formation	Growth
T (℃)	5.8 ± 3.2	7.1 ± 3.3	3.5 ± 5.8	5.3 ± 5.9
RH (%)	54 ± 22	52 ± 18	45 ± 17	46 ± 17
SO_2 (ppb)	16.7 ± 10.9	20.2 ± 13.0	2.6 ± 1.8	2.5 ± 1.5
NH_3 (ppb)	12.6 ± 18.0	11.2 ± 17.0	6.5 ± 9.5	6.6 ± 7.2
NO_2 + O_3 (ppb)	63.7 ± 8.4	70.1 ± 9.7	61.3 ± 14.0	63.8 ± 14.3
$PM_{2.5}$ (μg m^{-3})	56.5 ± 33.0	71.1 ± 49.0	30.3 ± 21.8	29.2 ± 20.4
SO_4^{2-} (μg m^{-3})	16.4 ± 11.0	18.5 ± 9.7	3.3 ± 2.4	3.6 ± 2.7
NO_3^- (μg m^{-3})	7.4 ± 5.7	7.4 ± 4.8	6.3 ± 5.1	6.7± 5.5
NH_4^+ (μg m^{-3})	5.5 ± 4.2	6.1 ±3.5	2.3 ± 1.7	2.2 ± 1.6
Calculated H_2SO_4 (10^7 molecules·cm^{-3})	8.8 ± 4.9	9.4 ± 4.5	2.2 ± 1.1	2.4 ± 1.0
$[H_2SO_4]_{avg}$/C (%)	59 ± 23	36 ± 18	23 ± 10	11 ± 7
TVOC (ppb)	7.0 ± 5.7[a]		16.1 ± 6 .5	
OC (μg m^{-3})	6.1 ± 3.0[b]		5.5 ± 2.0[c]	
EC (μg m^{-3})	1.8 ± 1.6 [b]		1.3 ± 0.6 [c]	

[a](Mao et al., 2009)

[b](Wang et al., 2011)

[c](Dong et al., 2020)